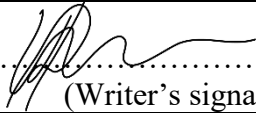




Faculty of Science and Technology

MASTER'S THESIS

Study program/Specialization: Petroleum Engineering - Master of Science Degree / Drilling Technology	Spring semester, 2016 <u>Open</u> / Restricted access
Writer: Artem Derusov	 (Writer's signature)
Faculty supervisor: Professor Alexander Yu Rozhko (IPT), Professor Muk Chen Ong (IKM) External supervisor(s):	
Thesis title: Effects of salt geometry on the overburden calculation for borehole stability study	
Credits (ECTS): 30	
Key words: Subsalt drilling, Geomechanics, Wellbore stability, Pore Pressure, Overburden Stress.	Pages:53..... + enclosure: Stavanger, ...28 jun /2016... Date/year

Abstract

Pre-drill pore pressure and fracture gradient predictions are important for successful drilling and well construction. There are numerous different methods for calculating the pore pressure in shales without direct measurements in the wellbore. All of the methods are based on interpretation of geophysical data, such as acoustic velocity and/or formation resistivity, which are sensitive to the effective stresses in the formation. Standard methods (like Bower's or Eaton's) utilize overburden effective stress for pore pressure prediction. Those methods are developed for regions with normal faulting stress regimes, where the direction of maximum compression is vertical and magnitude is equal to the weight of overburden. Due to the fluid-like behavior of salt on a geologic time scale, in situ stresses around salt structures may deviate significantly from regional tectonic directions, which in turn may significantly affect wellbore stability.

The main goal of this study is to quantify the difference in pore pressure and overburden stress predictions in a salt-related basin calculated with different methods, such as: a standard density integration and finite element modeling (FEM) using Plaxis software. The input geometry for geomechanical modeling was based on EDGE 2004 synthetic velocity model. The input geomechanical parameters were calculated from seismic interval velocity using empirical correlations developed for Gulf of Mexico.

In this study, it is demonstrated that a standard overburden calculation methods (based on density integration) can lead to errors in pore pressure prediction with magnitude up to 30 MPa; while 2D FEM is able to capture stress perturbation around salt structures. In majority of cases pre-drill developing of 3D FEM geomechanical model may not be feasible, because it is time consuming; while 2D geomechanical model is relatively quick and may significantly affect drilling decision to reduce the risk of well-bore instabilities caused by influx of formation fluids, losses of drilling fluid into formation, wellbore breakouts, tight hole intervals.

Acknowledgement

I would like to express special thanks to my supervisor, Prof. Alexander Yu Rozhko, for his continued support and guidance despite his busyness.

I owe my deepest gratitude to my co supervisor Prof. Muk Chen Ong, for his invaluable contribution. Without his support, I would not have made my thesis in time.

I also thank the Statoil ASA for the Plaxis software provided by them and for the free fruits in canteen.

In addition, I want to give thanks to Luis A. Rojo Moraleda, Alla Muminova, Roman Simonov, Romans Demcenko and Emil Gaizizulin, who spent their valuable time checking the grammar of my master thesis.

Table of contents

Abstract	i
Acknowledgement.....	ii
Table of contents	iii
List of Figures	v
List of Tables.....	vii
Abbreviations	viii
Symbols.....	ix
1 Introduction	1
2 Theory	4
2.1 Predicting wellbore stability	4
2.2 Mud weight window	4
2.3 Building geomechanical models.....	6
2.3.1 Relative stress magnitudes and faulting regimes	6
2.3.2 Overburden stress.....	7
2.3.3 Pore pressure	9
2.3.4 Minimum horizontal stress, S_{hmin}	11
2.4 Possible outcomes of wrong stresses prediction.....	11
2.5 About Finite element method (FEM)	12
2.6 About Plaxis 2D.....	13
3 Geomechanical modeling	14
3.1 Overview of the geomechanical model	14
3.2 Definition of geomechanical properties	15
3.3 Salt Properties.....	18
3.4 Setup the model in Plaxis	19
4 Results of simulation.....	21

4.1	Modeling magnitudes and directions of principal total stresses in the vicinity of salt structures	21
4.2	Principal total stresses along wellbore trajectories.....	24
5	Discussion of the results.....	27
5.1	Comparison of the overburden stress calculated by the 2-D method and the Finite element method	27
5.2	Comparison between the overburden stress calculated by the 2-D method and the 1-D method.....	29
5.3	Advantages and Disadvantages of methods which is used for creating the geomechanical model.....	30
5.4	Pore pressure calculated by Bower’s method.....	31
6	Conclusions	34
	References	35
	Appendix A. Definitions of the stress	39
	Appendix B. Mohr Coulomb model.....	40
	I. Young’s modulus (E) and Poisson’s ratio (ν)	40
	II. Cohesion (C), friction angle (ϕ) and angle of dilatancy (ψ).....	41

List of Figures

Figure 1.1 An explosion at a BP rig in the Gulf of Mexico.	2
Figure 2.1 Pressure in the borehole.....	5
Figure 2.2 E. M. Anderson’s classification scheme for relative stress magnitudes	7
Figure 2.3 Example of the density integration along the wellbore trajectory	8
Figure 2.4 Example of dividing the object into a subdomains.....	12
Figure 3.1 Cross section of the velocity model (m/s)	14
Figure 3.2 Seismic amplitudes plus seismic horizons cross section of the model	14
Figure 3.3 Lithographic cross section of the model	15
Figure 3.4 Calculated density for the model (sg).....	16
Figure 3.5 Calculated average density of different lithology for the model (sg).....	18
Figure 3.6 Lithographic model created in Plaxis	19
Figure 3.7 Pore pressure model created in Plaxis	20
Figure 4.1 Magnitudes and directions of principal total stress S_1 around the salt #1 (sg).....	22
Figure 4.2 Magnitudes of principal total stress S_2 around the salt #1 (sg).....	23
Figure 4.3 Magnitudes of principal total stress S_3 around the salt #1 (sg).....	23
Figure 4.4 Magnitudes and direction of principal total stress S_1 around the salt #2 (sg).....	23
Figure 4.5 Magnitudes of principal total stress S_2 around the salt #2 (sg).....	24
Figure 4.6 Magnitudes of principal total stress S_3 around the salt #2 (sg).....	24
Figure 4.7 Faulting regimes and direction of principal total stress S_1 around the salt #1	24
Figure 4.8 Faulting regimes and direction of principal total stress S_1 around the salt #2.....	24
Figure 4.9 Density model around the salt #1 (sg)	25
Figure 4.10 Magnitudes of principal total stresses and pore pressure along the well #1 (sg)..	26
Figure 4.11 Magnitudes of principal total stresses along the well #2 (sg).....	26
Figure 5.1 Magnitudes of maximum principal total stress S_1 calculated by Plaxis around the salt #1 (sg).....	27

Figure 5.2 Magnitudes of vertical stress S_{2D-v} calculated by 2D method around the salt #1 (sg)	27
Figure 5.3 Magnitudes of maximum principal total stress S_1 calculated by Plaxis around the salt #2 (sg)	27
Figure 5.4 Magnitudes of vertical stress S_{2D-v} calculated by 2D method around the salt #2 (sg)	27
Figure 5.5 Difference between 2D and FEM overburden stress calculations around the salt #1 (sg)	28
Figure 5.6 Difference between 2D and FEM overburden stress calculations around the salt #2 (sg)	29
Figure 5.7 Magnitudes of maximum principal stress along the wellpath #1 for three calculation methods	30
Figure 5.8 Magnitudes of maximum principal stress along the well-path #2 for three calculation methods	30
Figure 5.9 Density model at a distance from salts (sg)	31
Figure 5.10 Difference between 2D and FEM overburden stress calculations at a distance from salts (sg)	31
Figure 5.11 Difference between the pore pressure calculations in the salt #1 area (sg)	32
Figure 5.12 Difference between the pore pressure calculations in the salt #1 area (MPa)	32
Figure 5.13 Difference between the pore pressure calculations in the section #2 (sg)	32
Figure 5.14 Difference between the pore pressure calculations in the section #2 (MPa)	32
Figure 5.15 Difference between the pore pressure calculations in the well #1	33
Figure 5.16 Difference between the pore pressure calculations in the well #2	33
Figure A.1 (a) Stress tensor in Cartesian coordinates; (b) Tensor transformation through direction cosines; (c) The principal stress axes	39
Figure B.1 Mohr-Coulomb failure criterion	41

List of Tables

Table 2.1 Relative stress magnitudes and faulting regimes	6
Table 3.1 Parameters calculated for the each layer.	18
Table 3.2 Parameters for the Salt layers.....	19
Table 3.3 Input parameters for the pore pressure in Plaxis	20

Abbreviations

OVB	Overburden
FEM	Finite Element Method
1DM	1D Method
2DM	2D Method
sg	Specific gravity
2D_V	Vertical stress computed by density integration
MWW	Mud Weight Window
GoM	Gulf of Mexico

Symbols

K_0	Coefficient of lateral earth pressure (initial stress state)
ρ	Density
g	Acceleration due to gravity constant = 9,8m/s ²
σ'_v	Vertical effective stress
σ'	Effective stress
$\sigma, \sigma_{11}, \sigma_{22}, \sigma_{33}$	Normal stresses
$\tau_{12}, \tau_{21}, \tau_{13}, \tau_{31}, \tau_{23}, \tau_{32}$	Shear stresses
S_1, S_2, S_3	Principal total stresses
S_{OVB}	Overburden stress
S_V	Vertical stress,
S_{Hmax}	Maximum horizontal stress
S_{Hmin}	Minimum horizontal stress
S_C	Vertical stress of the point C
P_p	Pore pressure
Δt	Sonic transit time from well logging
Δt_n	Sonic transit time at the normal pressure,
V_p	Sonic velocity
V_{ml}	Compressional velocity
α	Biot coefficient
A and B	Calibrating parameters for the field
A_S and B_S	Fitting constants
C	Mudline transit time constants
D	Matrix transit time constants
P_{static}	Hydrostatic pressure
h	True Vertical Depth
$P_{dynamic}$	Hydrodynamic pressure
P_{pump}	Pump pressure
E	Young's modulus
ν	Poisson ratio
c	Cohesion
ϕ	Friction angle
α and β	Empirically derived constants. For most cases $\alpha=0,31$ and $\beta=0,25$
V_s	Shear wave velocity

φ	Porosity
ρ_{matrix}	Density of dry rock
ρ	Formation density
ρ_{fluid}	Density of the fluid
UCS	Unconfined compressive strength
ΔS	Difference of overburden stress
S_{2D_V}	Vertical stress is calculated by the 2D method
$P_{P_{S_1}}$	Pore pressure is calculated by uses S_1
$P_{P_{2D_V}}$	Pore pressure is calculated by uses S_{2D_V}
ΔP_P	Different between the pore pressures

1 Introduction

Instability of borehole is a main reason of borehole failures and represents a serious problem in the drilling industry (Zhang, 2013). Accurate wellbore stability analysis can prevent many problems, such as borehole washouts, breakout, collapse, stuck pipes and drill bits, losses of drilling fluid and fluid influx (kick). Instability of wellbore also increases a drilling time, increased costs, and may leads to loss of the well before it reaches its objective (Luo et al., 2012).

During the drilling, control of the mud density in the well is important to maintaining the wellbore stability (Charlez, 1999). Two major parameters determine the value of the density while drilling: the pore pressure, the fracture pressure (Glossary.oilfield.slb.com, 2016b). Pressure range between the pore pressure and the fracture pressure is called Mud Weight Window (Charlez, 1999). Static and dynamic pressures of the mud must be higher than the pore pressure and lower than the fracture pressure (Charlez, 1999). If the mud pressure is more than the fracture pressure, then it may lead to fracturing of the formation and losses of borehole fluids into formation. If it is less than the pore pressure, collapse or blowout may happen (Charlez, 1999; Zhang, 2011).

All methods for the pre-drill prediction of pore pressure and fracture pressure are based on the mathematical relationship between the overburden stress and the effective vertical stress (Zhang, 2011).

At the normal faulting regimes a maximum principal total stress is assumed to be vertical and equal to the weight of overlying formations (overburden stress) (Zoback, 2010). Thus, it can be calculated by integrating the density of the sediments overlying the depth of interest (Moos et al., 2003). The overburden stress for inclined boreholes can be calculated in two ways: integrating the density along the wellbore trajectory (using density logs) and integrating the density of the overlying rocks (Zoback, 2010). However, one of the key shortcoming for using of these methods is that it does not take into account perturbation of stresses around salt structures. Since the salt structure has a viscous nature and behaves like a fluid on geological time scale (Dusseault et al., 2004). The directions of principal stresses around salt structures may deviate significantly from regional tectonic directions (A. Rozhko et al., 2014).

Therefore, salt formations provide problems in to the design and construction of the often complex wells in deep water to be drilled in these locations (S. M. Willson et al., 2005).

Since a significant proportion of the world's hydrocarbon reserves are found in structures related to salt tectonics (Carlson et al., 2008), the errors in predicting mud weight windows can result to the failure of wells (S. Willson et al., 2003).

The BP Exploration & Production Inc. faced with the challenge of the wrong mud weight window prediction, which leads to the accident in the Gulf of Mexico (Bly, 2011).



Figure 1.1 An explosion at a BP rig in the Gulf of Mexico.

An obvious solution to prevent this problem is to use geomechanical models to simulate stresses around salt bodies (Luo et al., 2012). For the correct prediction of the overburden stress and creation the qualitative geomechanical model the simulation by the finite element method can be used (Fredrich et al., 2007).

The primary focus of this thesis is shows irregularity of the density integration method in contrast with the finite element method to computation the overburden stress in the region with salt structures.

We demonstrate that the pore pressure prediction is highly sensitive to the overburden calculation methods due to stress concentrations around salt structures that can cause a huge discrepancy in pore pressure prediction with magnitude up to 30 MPa.

The thesis is constructed as follows: First, we introduce a theoretical background for wellbore stability with short introduction to the pore pressure prediction methods. Next in geomechanical modeling section, we describe the preparation of the simulation model and the calculation of the main geomechanical parameters from seismic data. Simulation results, discussions and conclusions are presented in the end of thesis.

2 Theory

In this chapter we provide a brief introduction to the wellbore stability, pore pressure prediction methods and geomechanical modeling of stresses.

2.1 Predicting wellbore stability

Well drilling is commonly associated with time expenses and money (Bradley, 1978; Fredrich et al., 2007; McLean et al., 1990). To reduce the cost of drilling, it is very important to develop a good well design to avoid accidents and downtimes (Fredrich et al., 2003). One of the main conditions of careful development of well design is wellbore stability (Aadnoy et al., 2011). Wellbore stability is a function of mud weight and geomechanical properties (Aadnoy et al., 2011). The geomechanical parameters, such as stress, pore pressure and strength are difficult to estimate and remain the main issue (Huffman, 2002). Unfortunately there are limited numbers of options that can be used to minimize geomechanical stability problems (Aadnoy et al., 2011). Options include:

- Mudweight and mud type optimization.
- Optimization of casings.
- Optimization of well trajectory that likely will avoid drilling problems.
- Additionally, it may be also important minimize surge while running pipe and reduce a swab effect.

In order to make a better result and maximize the number of possible solutions geomechanical design restrictions must be developed as soon as possible in the field life (Zoback, 2010). In this way, field production can be reducing the number of problematic wells and facility costs.

2.2 Mud weight window

Drilling mud is a most important component for saving the stability of wellbore. The drilling mud helps to clean the hole from the cuttings by transporting them to the surface. It lubricates the drill string. The mud supports and stabilizes the wellbore wall from collapse. It also balances formation pressures in the well to reduce the risk of kick or blowout (Glossary.oilfield.slb.com, 2016b).

One of the key parameters of the mud is mud weight. Mud weight is selected considering the pore and fracture pressures around the well (Charlez, 1999). The hydrostatic pressure could be calculated by the formula below.

$$P_{static} = \rho gh \tag{2.1}$$

Where P_{static} is a hydrostatic pressure of the mud [Pa], ρ is a mud weight [kg/m³], h is a True Vertical Depth [m], and g is the acceleration due to gravity [9.8 m/s²]

For the calculation of the hydrodynamic pressure is required to add pump pressure to the hydrostatic pressure.

$$P_{dynamic} = P_{static} + P_{pump} \tag{2.2}$$

Where $P_{dynamic}$ is a hydrodynamic pressure of the mud [Pa], and P_{pump} is a pump pressure [Pa]. Hydrostatic and hydrodynamic pressures of the mud (red curve) must be higher than the pore pressure (green curve) and lower than the fracture pressure (blue curve) (see Figure 2.1).

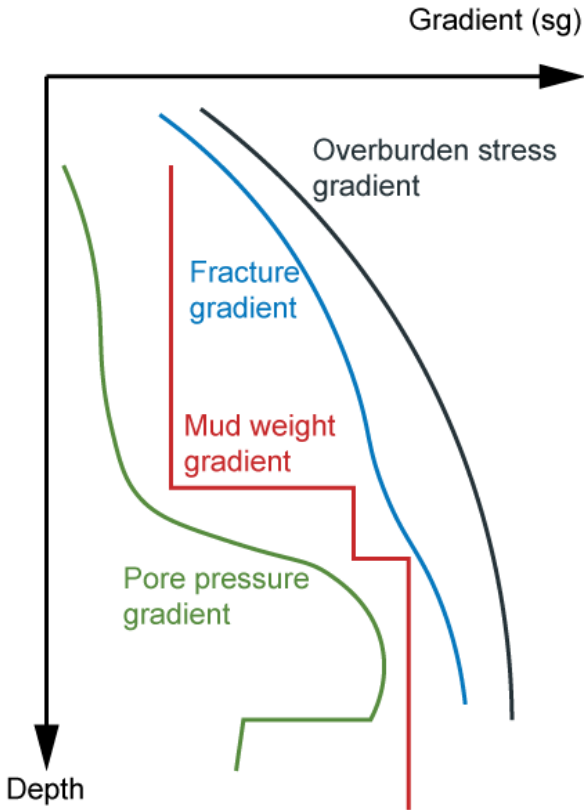


Figure 2.1 Pressure in the borehole

The gap between the pore pressure and the fracture pressure is called a mud weight window. The safe mud weight is selected to minimize the risk of the wellbore problem.

2.3 Building geomechanical models

The basic elements of the geomechanical models for wellbore stability analysis are:

- The rock properties, including strength
- The state of the stress (the orientation and magnitude of the principal stress)
- The pore pressure.

All of these parameters are necessary to create the qualitative design of the wellbore. Another information important for the wellbore stability is an information about chemo-physical properties of shales and how shales will interact with various drilling fluids (Darley et al., 1988). Here we leave outside of the scope of this thesis investigations of chemical effects of mud on shale stability.

2.3.1 Relative stress magnitudes and faulting regimes

To predict the wellbore stability, the principal stress of the rock is used. The vertical stress can be the greatest, the intermediate, or the least principal stress. The relationship between magnitudes and the directions of the principal stress (S_1, S_2, S_3) for the most geomechanical models are defined by (Anderson, 1951):

Table 2.1 Relative stress magnitudes and faulting regimes

Regime	Stress		
	S_1	S_2	S_3
Normal	S_V	S_{Hmax}	S_{Hmin}
Strike-slip	S_{Hmax}	S_V	S_{Hmin}
Reverse	S_{Hmax}	S_{Hmin}	S_V

If the vertical stress is the greatest stress, than it is a normal faulting regime, as shown in Table 2.1 and Figure 2.2. When the vertical stress is the intermediate stress, a strike-slip regime is presented. If the vertical stress is the least stress the regime is defined to be reverse. (Aadnoy et al., 2011; Zoback, 2010).

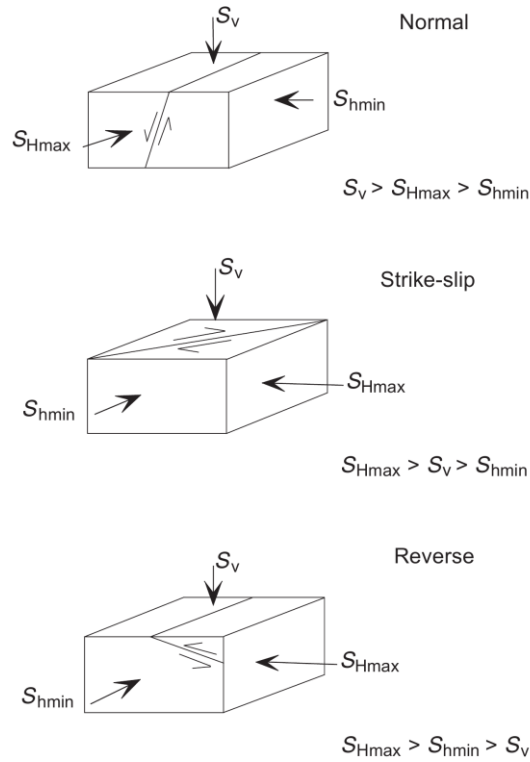


Figure 2.2 E. M. Anderson's classification scheme for relative stress magnitudes

2.3.2 Overburden stress

The overburden stress is equal to the maximum principal total stress (Zoback, 2010). In the normal faulting regime it is equivalent to the weight of overlying formations (2.3) and can be called the vertical stress (Zoback, 2010),

$$S_v(z) = p_0 + g \times \int_0^z \rho(z) dz \quad (2.3)$$

where S_v is vertical stress, ρ is density of the rock in the cell, z is depth and g is gravity.

There are several techniques for calculation the vertical stress in the well: by integration of density along wellbore trajectory (1D-method), by vertical integration of density along wellbore trajectory (2D method) and by geomechanical method, using finite element or other modeling techniques (Aadnoy et al., 2011). 2D methods is more appropriate for inclined boreholes, because the density above borehole may not be the same as density along wellbore, as shown on Figure 2.3. While 2D density integration method does not take into account the redistribution of stresses inside and outside of salt structures, which may significantly deviate from regional stress directions and magnitudes (Matthews et al., 1967).

Figure 2.3 displays an example of a geological cross-section. Red line represents the well path. Brown and Green solids represent the formation layers with different weight. Yellow line represents a vertical load on the point C.

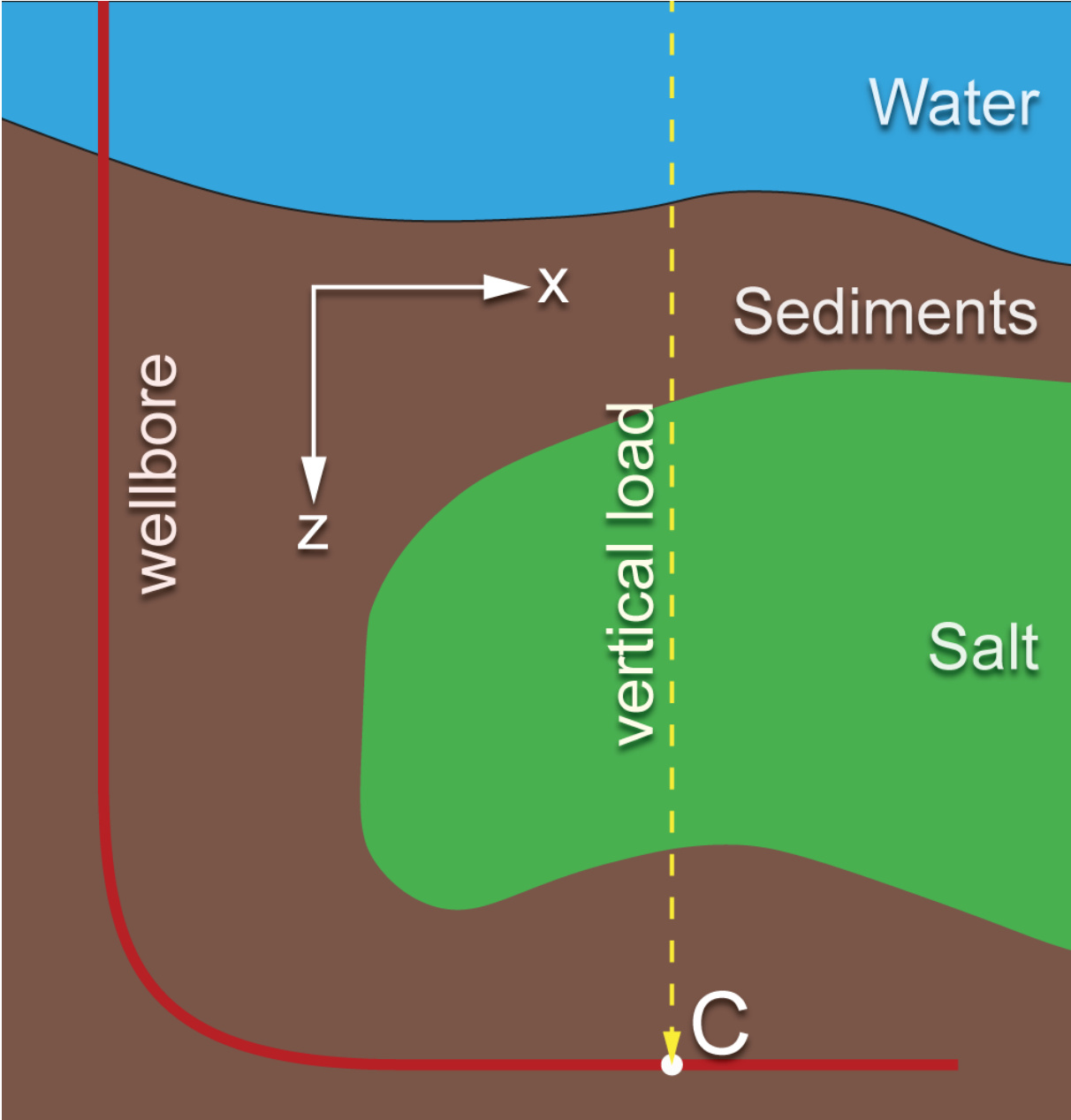


Figure 2.3 Example of the density integration along the wellbore trajectory

Vertical load calculated by 2-D method in the point C at Figure 2.3, is equal to

$$S_C = g \times \int_{vertical(z)} \rho(x; z) dz \times h_{cell} \tag{2.4}$$

Where ρ is density of the rock in the cell [kg/m³] and h_{cell} is a height of cell [m].

For the 1-D method, the vertical stress of the point C in Figure 2.3 is calculated by the equation (2.5)

$$S_C = g \times \int_{wellbore(x;z)} \rho(x; z) dz \times h_{cell} \quad (2.5)$$

In the real life the density data, used in computing the vertical stress, can be obtained from the seismic velocity log using the empirical correlation (Gardner et al., 1985; Zoback, 2010). These equations are based on standard equations with unknown coefficients, which are defined individually for each field. Coefficients are determined by comparing the real data from exploration wells and data obtained by formulas.

However, the direction and magnitude of maximum principal total stress can change near the salt formations area (Bradley, 1978; Fredrich et al., 2003), because the salt structure has a viscous nature and behaves like a fluid on geological time scale (Dusseault et al., 2004). For this case, the finite element method is used to calculation of the magnitude and direction of the maximum principal total stress in the well (see chapter 2.5).

2.3.3 Pore pressure

Pore pressure is the pressure of the fluid contained in the pore space at a specific depth (Zoback, 2010). Without any other geophysical processes, the pore pressure is equivalent to the hydrostatic pressure. However, geophysical processes in the rock, such as disequilibrium compaction, heat expansion of water, fluid density contrasts, chemical transformations, etc., can contribute to the overpressure generation (Zoback, 2010).

There are only three ways to determine pore pressure for new wells. There are pre-drill pore pressure prediction, pore pressure prediction while drilling and post-well pore pressure analysis (Aadnoy et al., 2011).

Pre-drill and while-drill pore pressure in shales can be predicted using the seismic velocity data of the field and using acoustic and resistivity logs. It includes those techniques as Eaton's method, Bower's method, and Tau model (Gholami et al., 2014).

The pore pressure is an important geomechanical parameter for the mud weight computation (Zhang et al., 2008). There are a large number of methods that can be used to evaluate the pore pressure based on other measurements (Sayers et al., 2002).

All methods for the pre-drill prediction of pore pressure are based on the mathematical relationship between the pore pressure and the effective stress (Zhang, 2011).

$$\sigma'_V = (S_{OVB} - \alpha P_P) \quad (2.6)$$

Where σ'_v is the vertical effective stress, S_{OVB} is the overburden stress, P_p is the pore pressure, and α represent the Biot effective stress coefficient, typically taken as $\alpha=1$ in geoscience community (Biot et al., 1957).

Eaton uses empirical equation to predict the pore pressure gradient from sonic compressional transit time (Zhang, 2011).

$$P_p = S_{OVB} - (S_{OVB} - P_h) \left(\frac{\Delta t_n}{\Delta t} \right)^3 \quad (2.7)$$

Where P_p is a pore pressure, P_h is hydrostatic pore pressure, S_{OVB} is overburden stress, Δt_n is the sonic transit time at the normal pressure, and Δt is the sonic transit time from well logging. This method does not consider the unloading effects.

Bower considers that the vertical effective stress (σ'_v) and sonic velocity (V_p) have following relationship (Zhang, 2011):

$$V_p = V_{ml} + A \times \sigma'_v{}^B \quad (2.8)$$

Where V_{ml} is the compressional velocity, A and B are the calibrating parameters for the field. Transform the equation (2.8) with considering equation (2.7) to

$$P_p = S_{OVB} - \left(\frac{V_p - V_{ml}}{A} \right)^{\frac{1}{B}} \quad (2.9)$$

This method is applicable to many deposits (e.g., the Gulf of Mexico). However, it does not work with formations with slow velocities.

Tau model is similar to Bower's method, It is base uses relationship between effective stress (σ_e) and the compressional transit time (Δt).

$$\sigma_e = A_S \times \left(\frac{C - \Delta t}{\Delta t - D} \right)^{B_S} \quad (2.10)$$

Where A_S and B_S are the fitting constants, C and D are the mudline and the matrix transit time constants respectively. The equation (2.10) together with the equation (2.7) are transformed to

$$P_A = \sigma_{OVB} - \left(\frac{C - \Delta t}{\Delta t - D} \right)^{B_S} \quad (2.11)$$

Tau model, compared with Bower's method, considers the mudline and matrix velocities effects (Zhang, 2011).

These methods were developed only for shales which helps geoscientist to estimate the most likely pore pressure in the sandstone formations for new fields.

Pore pressure in salt structures is not defined, because salt is a non-porous material at depth. While salt structures may contain inclusions of porous sediments (Whitson et al., 2001). The pore pressure in those sediment inclusions can be as high as overburden stress in salts.

Next way is a prediction of the pore pressure while the drilling. In this case, the pore pressure is measured during the well drilling. It is based on the analysis of the measurement and logging while drilling, drilling parameters and data from the mud (Zhang, 2011). And the last way is post-well pore pressure prediction. This method measures the pore pressure in the drilled well, and uses this data for the future nearby wells (Zhang, 2011).

2.3.4 Minimum horizontal stress, S_{Hmin}

Fracture pressure, is a pressure at which fracturing of the formation occurs while drilling (Aadnoy et al., 2011). Fracturing of the formation while drilling can cause losses of drilling fluid into formation or in the extreme case it may cause leakage of hydrocarbon into the overburden. It can be calculated from the minimum stress. Usually, the minimum stress is the lower bound of the fracture pressure (Zhang, 2013). It can be predicted by simulation (for new field), or can be measured directly by extended leakoff tests or minifrac tests (Haimson et al., 2003). Also, using the uniaxial strain model, the minimum stress can be calculated if the overburden stress, pore pressure and Poisson's ratio are known (Zhang, 2011). In a normal faulting stress regime, the minimum horizontal stress is the minimum principal in-situ stress (Zoback, 2010). Eaton (1969) proposed an empirical expression (2.12) for the magnitude of the minimum horizontal stress S_{Hmin} as a function of depth in the Gulf of Mexico region.

$$S_{Hmin} = \left(\frac{\nu}{1 - \nu} \right) (S_{OVB} - P_p) + P_p \quad (2.12)$$

Where ν is a Poisson ratio, S_{OVB} is the overburden stress and P_p is a pore pressure.

Subsequently, the predicted stresses are used for mud weight calculation. Similar methods, but with different coefficients in front of $(S_{OVB} - P_p)$ in equation (2.12) were proposed by Hubbert et al. (1972); Matthews et al. (1967) and other authors.

2.4 Possible outcomes of wrong stresses prediction

The pore pressure and the fracture pressure are closely linked to the overburden stress, as mentioned above. Wrong prediction of the overburden stresses leads to incorrect calculations of the pore pressure and fracture pressure (Charlez, 1999; Zhang, 2011) and it increases the probability of going beyond the mud weight window boundaries.

If the mud pressure is higher than the fracture pressure, then it can lead to fracturing of the formation and the circulation lost. On the other hand, if it is less than the pore pressure, collapse, kicks or blowout may occur (Charlez, 1999; Zhang, 2011).

From 1993 to 2002 2520 gas wellbores were drilled in the Gulf of Mexico. More than 24% of non-productive time was associated with inaccurate calculations of the pore pressure and the fracture pressure (Dodson et al., 2004).

Therefore, correct computations of the overburden stresses are important to reduce the non-productive time and avoid drilling incidents.

2.5 About Finite element method (FEM)

The finite element method (FEM) is a numerical technique developed to find approximate solutions to boundary value problems of partial differential equations (Zienkiewicz et al., 2005)

The first step of this method is dividing the studied object into a collection of subdomains (Figure 2.4). Each subdomain contains a set of element equations coming from the original problem. The number of equations equals to the number of unknown values at the nodes. It is directly proportional to the number of elements, and is limited only by the capacities of the computer (Bathe, 2008).

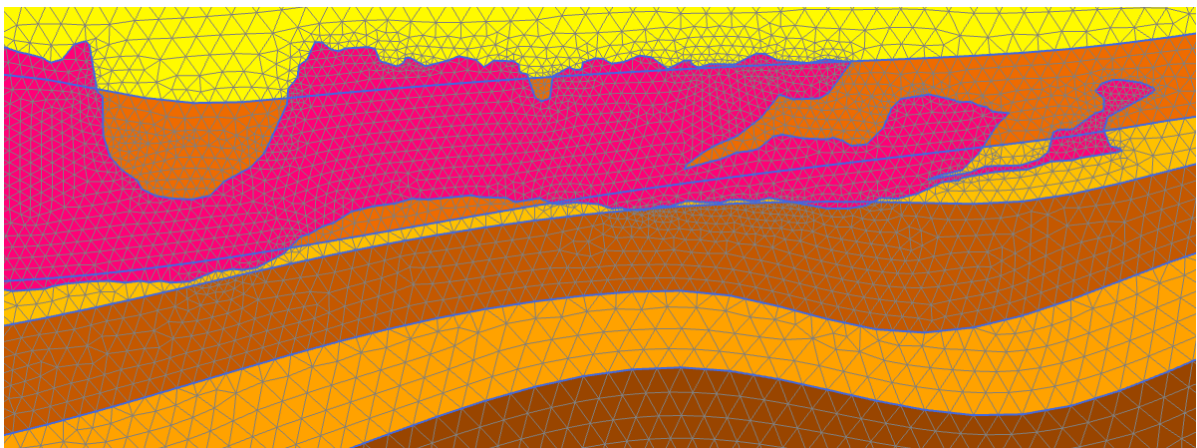


Figure 2.4 Example of dividing the object into a subdomains

The second step of FEM is to solve the all element equations by comparing the element equations at the subdomains boundaries. The found values at the boundaries of subdomains are the solutions of the problem.

2.6 About Plaxis 2D

In this master thesis we use Plaxis to calculate stresses around salt structures in 2D and along wellbore trajectories.

“PLAXIS is a finite element program for geotechnical applications in which soil models are used to simulate the soil behavior” (Brinkgreve et al., 2015). It is a package of the Computational programs for the finite element calculation of geotechnical problems. This software package is also widely used in Petroleum industry for simulation around salt bodies (A. Rozhko et al., 2014) and in the overburden during reservoir depletions (Røste et al., 2015).

It is a package of the computational programs for the finite element calculation of geotechnical problems.

In the software package PLAXIS a formation is simulated as a multicomponent material, in which pore pressure can be predefined as an input parameter for geomechanical modeling.

The basic soil model is the model of Mohr-Coulomb (Brinkgreve, 2005). It based on the five input parameters: i.e. Young’s modulus (E) and Poisson ratio (ν), for soil elasticity; friction angle (ϕ) and Cohesion (C) for soil plasticity and angle of dilatancy (ψ) as an angle of dilatancy (more details can be found in the Appendix B).

3 Geomechanical modeling

This chapter describes the preparation of the simulation model and the calculation of the main geomechanical parameters.

3.1 Overview of the geomechanical model

In this study, a synthetic 2D velocity model of the field is considered (see Figure 3.1). The velocity model was created by Billette and Brandsberg-Dahl (Billette et al., 2005). This model has been used for simulations in companies such as BP, Schlumberger, Statoil etc (Cavalca et al., 2015)

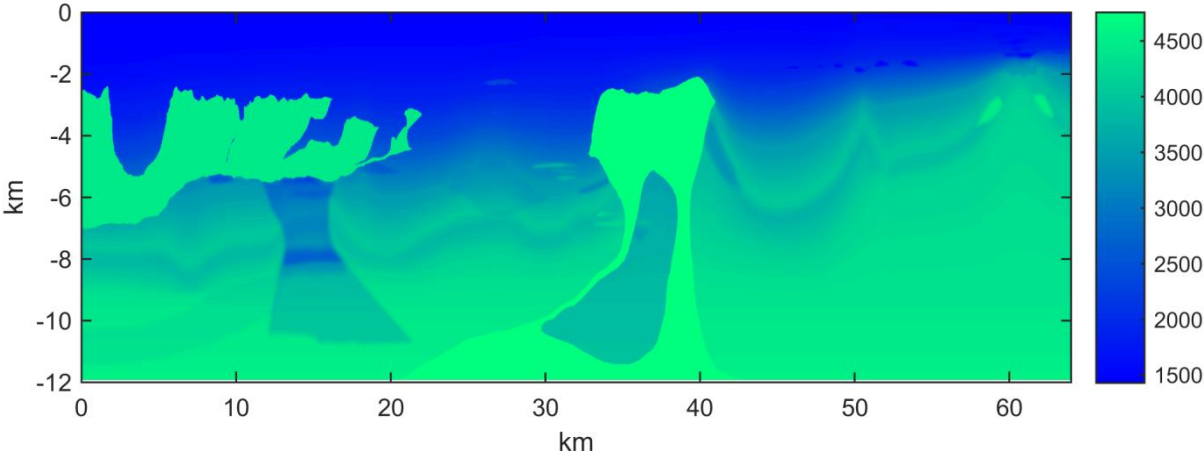


Figure 3.1 Cross section of the velocity model (m/s)

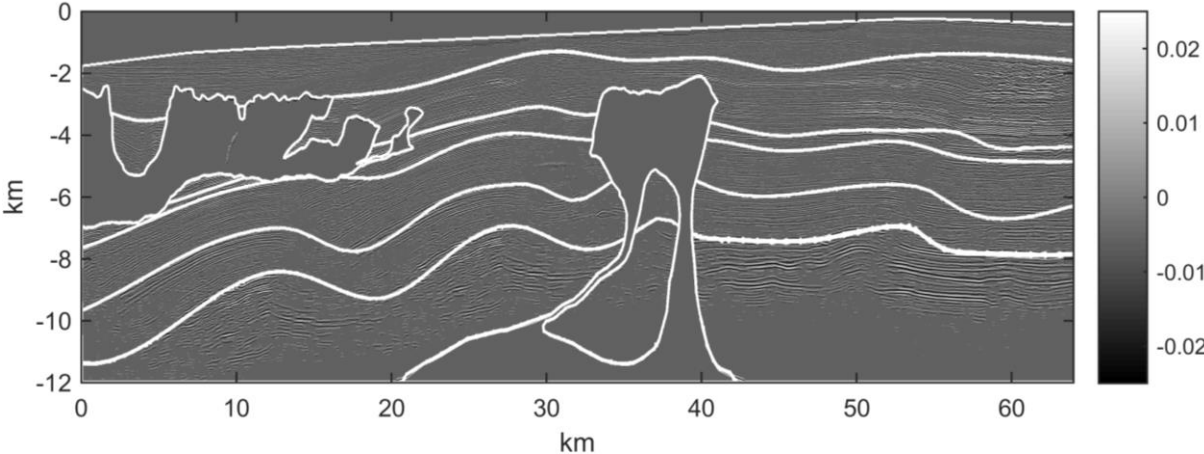


Figure 3.2 Seismic amplitudes plus seismic horizons cross section of the model

The 2D velocity model has a depth of 12 km and a length of 64 km. The model is a synthetic analog of salt structures observed in the Gulf of Mexico and West Africa.

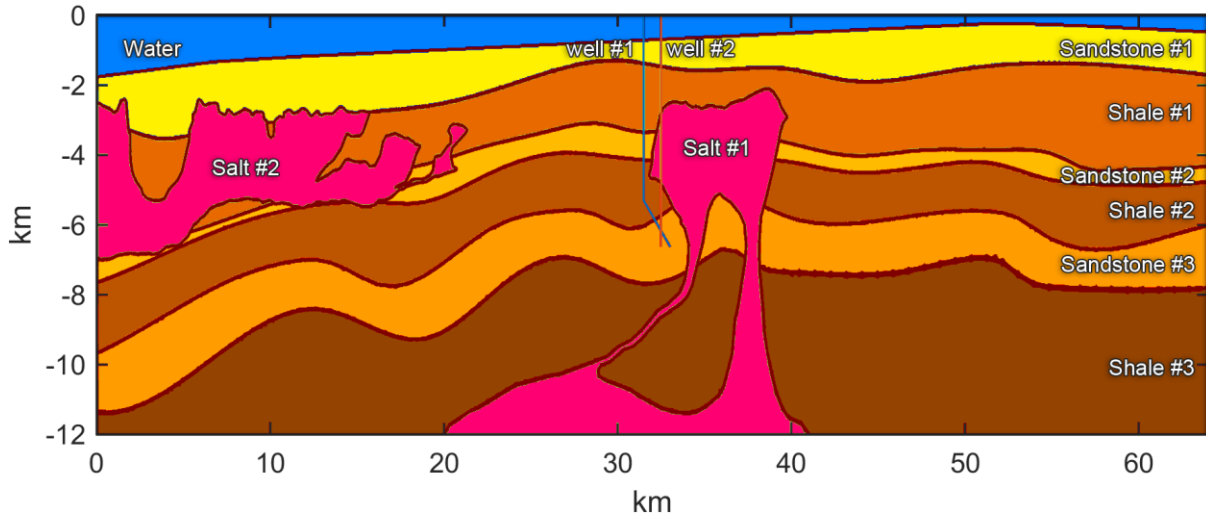


Figure 3.3 Lithographic cross section of the model

In the model, shown in Figure 3.3, one can see three sandstone formations, three shale formations and two salt structures. One of the salt domes is located in the center of the 2D model (salt #1). The other one is on the left side of the model (salt #2).

Furthermore on the Figure 3.3 2 well trajectories can be observed. Trajectory of Well #1 is placed near to the salt formation and has one build section. Well #2 is vertical and penetrates through the salt structure #1.

3.2 Definition of geomechanical properties

Input parameters from the different layers such as density, Young's modulus, Poisson's ratio, cohesion and friction angle are required to calculate the stress using the finite element method. Empirical correlations are used for determination of input parameters for different layers from interval velocity model.

Gardner's relation is used to calculate the density from V_p velocity (Gardner et al., 1985)

$$\rho = \alpha V_p^\beta \quad (3.1)$$

Where ρ is density given in g/cm^3 , α and β are empirically derived constants, and V_p is velocity of P-wave given in m/s. For most cases $\alpha=0.31$ and $\beta=0.25$, and the equation is reduced to:

$$\rho = 0.31 \times V_p^{0.25} \quad (3.2)$$

After performing the calculations, the following density values were obtained (see Figure 3.4)

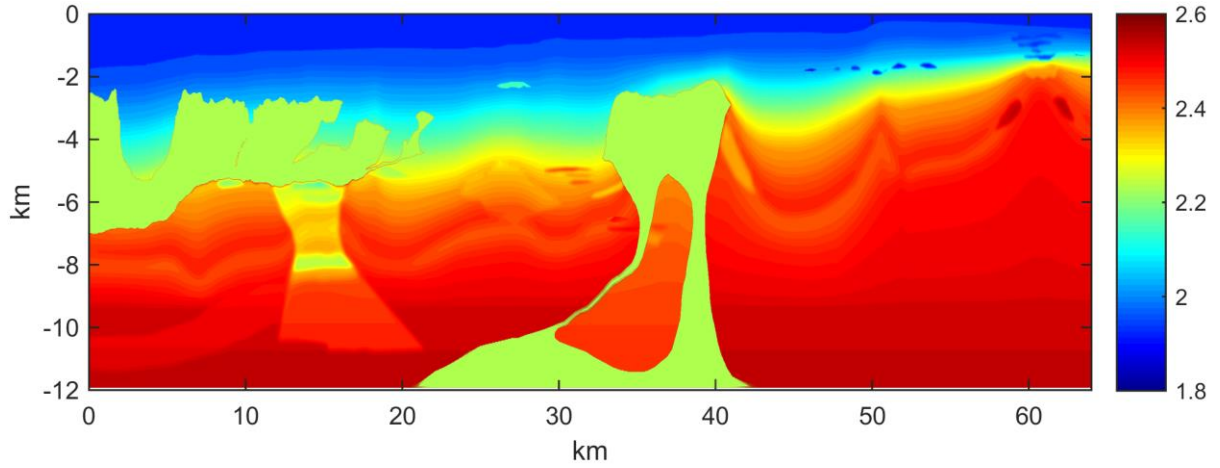


Figure 3.4 Calculated density for the model (sg)

For calculating shear wave velocity Castagna's equation is used (Castagna et al., 1985)

$$V_p = 1.16 \times V_s + 1.36 \quad (3.3)$$

Where V_p is P-wave velocity, and V_s is S-wave velocity in km/s. By derivation of V_s from the formula and converting it from km/s to m/s the formula is obtained (3.4).

$$V_s = \frac{V_p - 1360}{1.16} \quad (3.4)$$

Where V_p and V_s in m/s.

Young's modulus is determined from equation (3.5) (Mavko et al., 2009)

$$E = \frac{\rho V_s^2 (3V_p^2 - 4V_s^2)}{V_p^2 - V_s^2} \quad (3.5)$$

Where E is Young's modulus in Pa, ρ is density given in kg/m^3 , and V_p and V_s are referred as P-wave and S-wave velocities in m/s, respectively.

Poisson's ratio (ν) can be expressed as shown below (Glossary.oilfield.slb.com, 2016a)

$$\nu = \frac{1}{2} \frac{(V_p^2 - 2V_s^2)}{(V_p^2 - V_s^2)} \quad (3.6)$$

Equation (3.7) is an empirical relationship between P-wave velocity (V_p [m/s]) and internal friction angle (ϕ [°]) for shale (Chang et al., 2006)

$$\phi = \sin^{-1} \left(\frac{V_p - 1000}{V_p + 1000} \right) \quad (3.7)$$

For sandstone internal friction angle is calculated by equation (3.8)

$$\phi = 57.8 - 105\varphi \quad (3.8)$$

Where φ is the porosity of sandstone, determined from the formula (3.9)

$$\phi = \frac{\rho_{matrix} - \rho}{\rho_{matrix} - \rho_{fluid}} \quad (3.9)$$

Where ρ_{matrix} is the density of dry rock, ρ is the formation density (3.2), and ρ_{fluid} is fluid density. For given case for all sandstone formations $\rho_{matrix}= 2650 \text{ kg/m}^3$ and $\rho_{fluid}= 1000 \text{ kg/m}^3$.

Next step is to determine Unconfined Compressive Strength (UCS). UCS is required to calculate Cohesion. For sandstone UCS is equal to (Chang et al., 2006):

$$UCS = 3.87e^{1.14 \times 10^{-10} \rho V_p^2} \quad (3.10)$$

Where ρ is the density given in kg/m^3 , and V_p is P-wave velocity in m/s

For shale UCS is equal to (Chang et al., 2006):

$$UCS = 0.5 \times \left(\frac{304.8 V_p}{3.2 \times 10^{-6}} \right)^3 \quad (3.11)$$

Where UCS is the unconfined compressive strength in MPa, and V_p is the P-wave velocity in m/s .

Cohesion (C [MPa]) is derived from the uniaxial compression in Mohr-Coulomb equation (3.12) (Rocscience.com, 2016).

$$\frac{UCS}{2} = \frac{UCS}{2} + C \times \cos(\phi) \quad (3.12)$$

$$C = \frac{UCS}{2} \times \frac{1 - \sin(\phi)}{\cos(\phi)} \quad (3.13)$$

Where UCS is the unconfined compressive strength in MPa, and ϕ is the internal friction angle in degrees.

After performing the calculations the following average values for each layer were obtained as follows (Table 3.1).

Table 3.1 Parameters calculated for the each layer.

		1 st layer	2 nd layer	3 rd layer	4 th layer	5 th layer	6 th layer
Formation type		Sandstone	Shale	Sandstone	Shale	Sandstone	Shale
V _p	m/s	1636.84	2556.49	3437.53	3812.98	4031.34	4393.74
V _s	m/s	238.66	1031.46	1790.98	2114.64	2302.88	2615.29
ρ	kg/m ³	1971.80	2204.31	2373.69	2436.00	2470.15	2523.89
φ		0.41	-	0.17	-	0.11	-
E	GPa	0.33	6.58	20.00	27.84	32.95	42.32
ν		0.389	0.3	0.314	0.278	0.258	0.226
ϕ	°	14.64	25.95	40.22	35.76	46.36	38.99
C	MPa	2.73	2.42	18.97	6.59	25.29	9.39

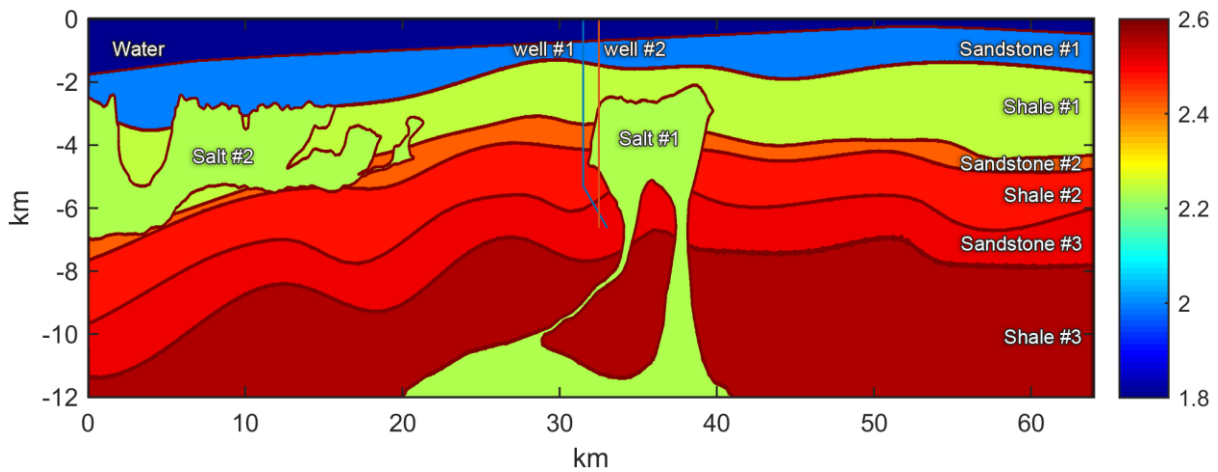


Figure 3.5 Calculated average density of different lithology for the model (sg)

3.3 Salt Properties

Salt has a viscous nature and behave like a fluid on geological time scale. Therefore shear stress cannot exist in the salt. Plaxis cannot use zero values for the cohesion and the friction angle properties (Brinkgreve et al., 2015). Therefore, zero values for cohesion and friction angle are substituted for the smallest possible values at which the calculations will be converged. Parameters for salt structures were taken from Luo et al. (2012).

Table 3.2 Parameters for the Salt layers.

Formation type		Sandstone
ρ	kg/m ³	2200.00
E	GPa	3.1
ν		0.25
ϕ	°	0.35
C	MPa	0.001

3.4 Setup the model in Plaxis

Lithographic model is created in Plaxis (see Figure 3.6), which uses parameters for soils from Table 3.1 and Table 3.2

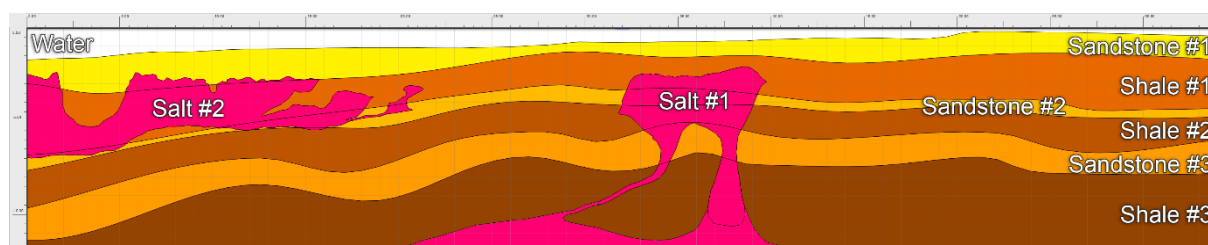


Figure 3.6 Lithographic model created in Plaxis

The plane strain model is used to describe the 2D cross-section. The computational domain used for the analysis has a measure 64x12 km. Left and right borders is a slip boundaries. The borderline between the water and sandstone #1 layers is a free surface.

The water density is 1000 kg/m³. Gravity is 1.0g or 9.81 m/s² and has -Y direction. The initial stresses in the model are geostatic. For the sediments a horizontal-to-vertical stress ratio is $K_0=0.7$ and for the salt $K_0=1$ (Nikolinakou et al., 2014). For the initial phase, calculation type is set to “gravity load”. The next phases “plastic” calculation type is used.

Input pore pressure model is based on the prediction of the pore pressure by Bowers method. The water condition for clusters is shown in Table 3.3. Pore pressure calculation is set to “phreatic” for the initial phase, and uses “pressure from previous stage” for the next phases.

Table 3.3 Input parameters for the pore pressure in Plaxis

Layer number	Type of layer	Water head level (km)
1 st layer	Sandstone #1	0
2 nd layer	Shale #1	interpolated pore pressure
3 rd layer	Sandstone #2	1.8
4 th layer	Shale #2	interpolated pore pressure
5 th layer	Sandstone #3	3.0
6 th layer	Shale #3	interpolated pore pressure
Bottom	boundary	9.5

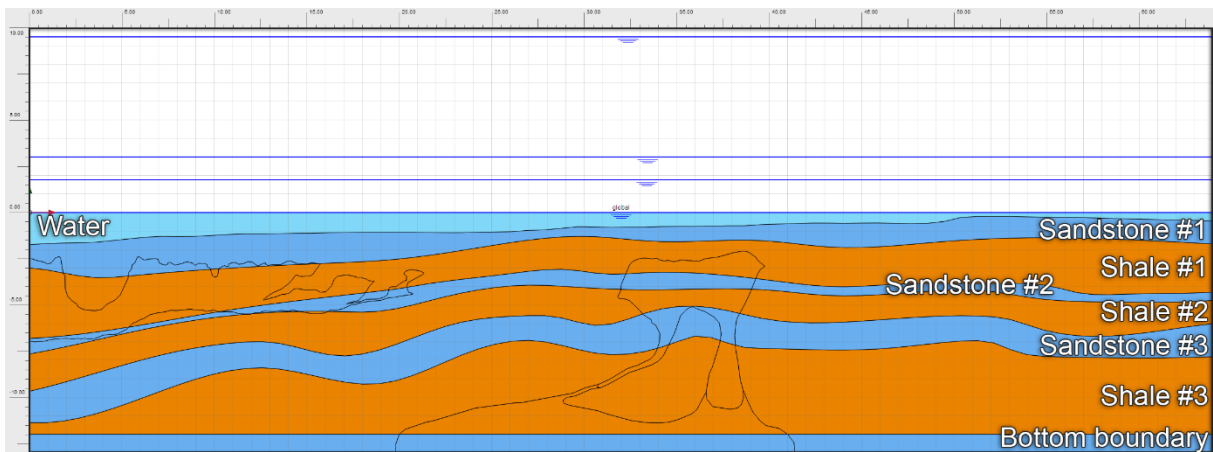


Figure 3.7 Pore pressure model created in Plaxis

4 Results of simulation

In order to present the results computed by Plaxis in a convenient format, we developed a Matlab code in this thesis. This code converts simulation results from Plaxis into the specific gravity data plot. Most of the figures were plotted by Matlab R2014b.

The specific gravity (sg) shows how many times pressure is larger than hydrostatic water pressure at the same depth. It is used to help to understand what mud density is required at given depth. The density of fresh water is 1 sg, which is equal to 1000 kg/m^3 . This has been performed to get a better understanding about the required mud density at a given depth.

4.1 Modeling magnitudes and directions of principal total stresses in the vicinity of salt structures

This section displays the 2D calculations for magnitude and directions of principal stresses around salt structures.

The color in Figure 4.1, Figure 4.2, Figure 4.3, Figure 4.4, Figure 4.5 and Figure 4.6, shows the magnitude of principal stresses in the sg units. Red contours show the boundary of formations on the figures. Lines in Figure 4.1 and Figure 4.4, illustrate the orientation of principal stresses. As salt, acts like a fluid on geological time scale, all principal stresses are almost identical (Nikolinakou et al., 2012). Because of this the shear stresses cannot exist in the salt, directions of the total principal stresses are not defined in salt and not shown.

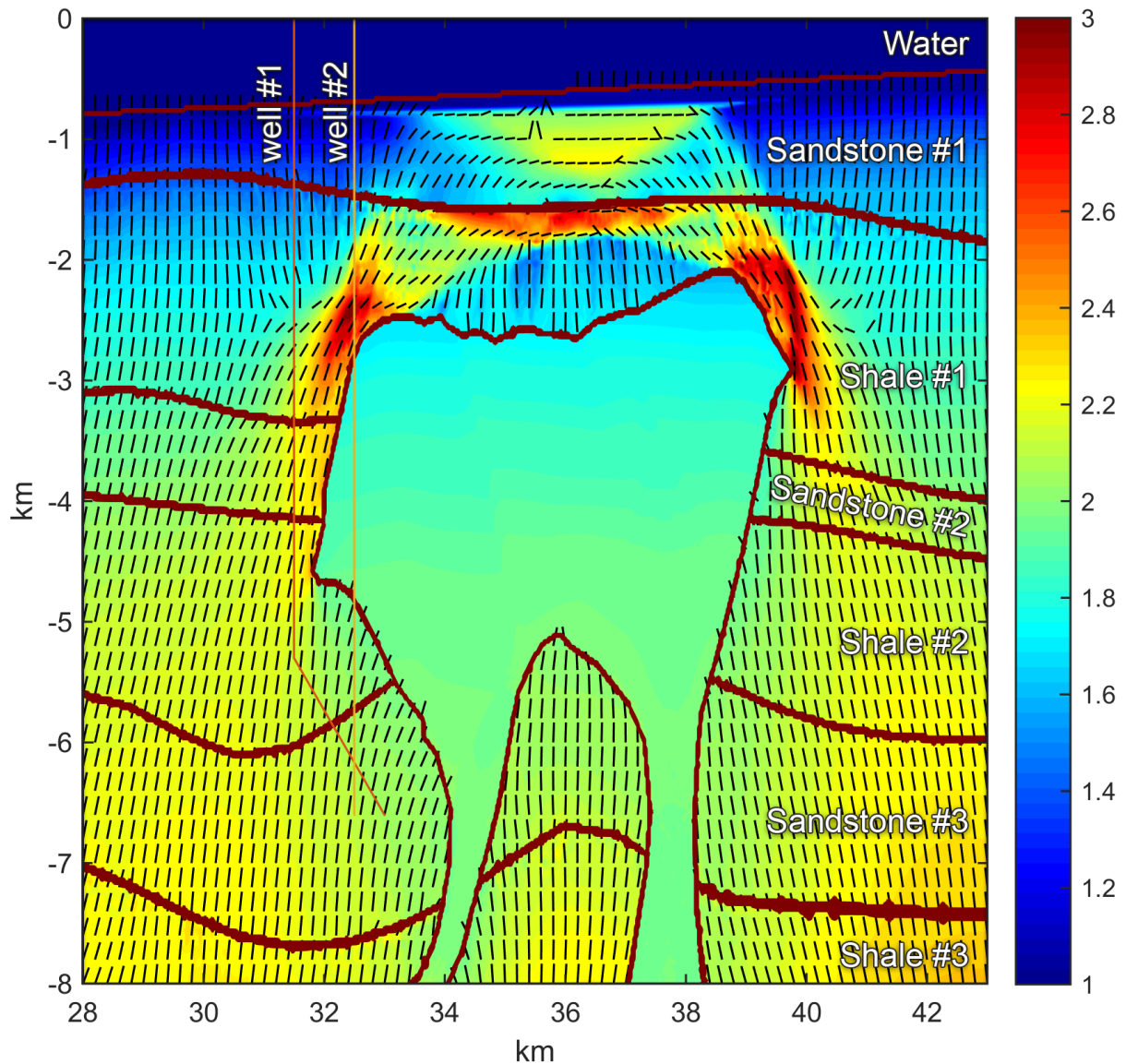


Figure 4.1 Magnitudes and directions of principal total stress S_1 around the salt #1 (sg)

Rise of principal total stress associated with the depth increase can be seen at the Figure 4.1. The highest values of the principal total stress are on sharp corners of the salt boundaries. It is associated with the concentration of stresses in these points. The same is observed in Figure 4.2 and Figure 4.3. All principal total stresses in the salt are almost identical. All principal total stresses near the salt boundary are either parallel or perpendicular to the salt surface, because there are no shear stresses on the salt surface.

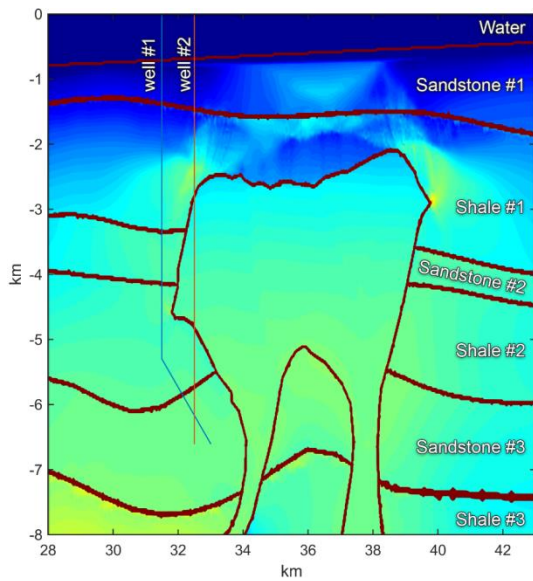


Figure 4.2 Magnitudes of principal total stress S_2 around the salt #1 (sg)

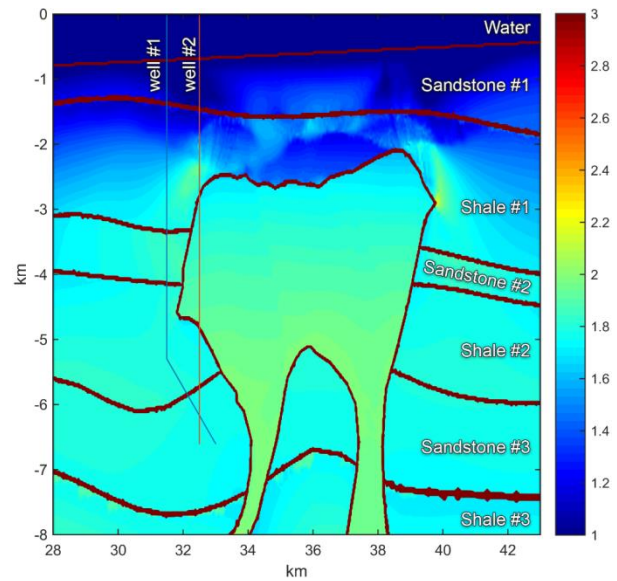


Figure 4.3 Magnitudes of principal total stress S_3 around the salt #1 (sg)

Distribution of the horizontal principal stress near the salt Figure 4.4 is more homogeneous (see Figure 4.2 and Figure 4.3). However the highest values of the principal total stresses are on sharp corners of the salt boundaries. The S_2 and S_3 in the salt are higher than stresses that are located around.

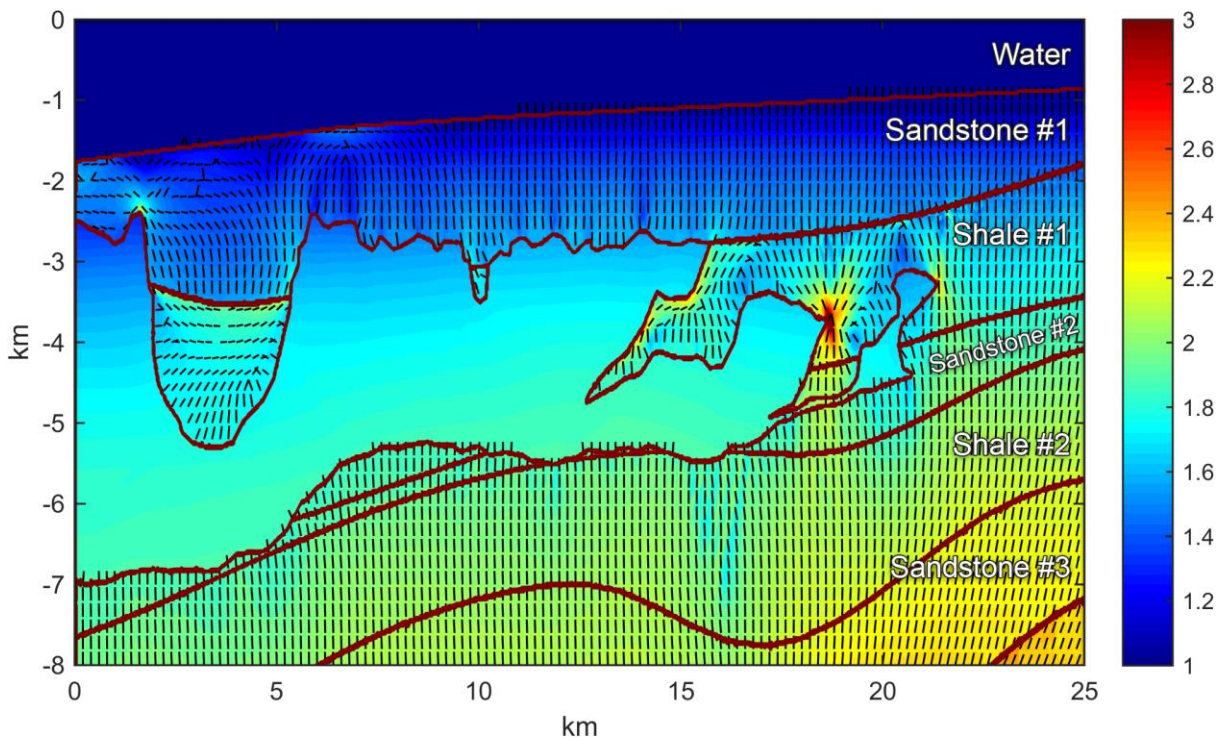


Figure 4.4 Magnitudes and direction of principal total stress S_1 around the salt #2 (sg)

On Figure 4.4, Figure 4.5 and Figure 4.6 it is easy to notice that there are large concentration of stress taking place on the sharp corners of the salt boundaries. Also, the high values of the maximum total principal stress are at places where the directions of S_1 changes abruptly. All

principal total stresses in the salt have practically identical values. Maximum compressive stress is re-orientated near salt structure, but at a distance from salt it is oriented vertically.

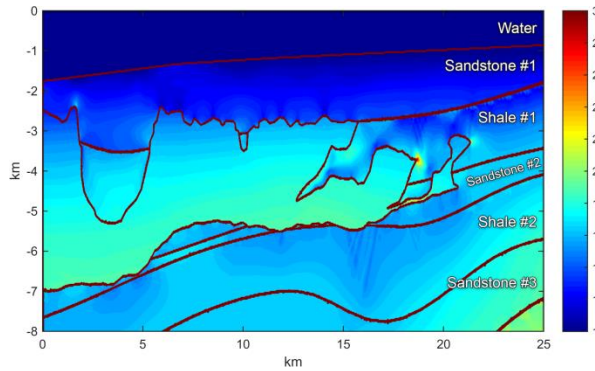


Figure 4.5 Magnitudes of principal total stress S_2 around the salt #2 (sg)

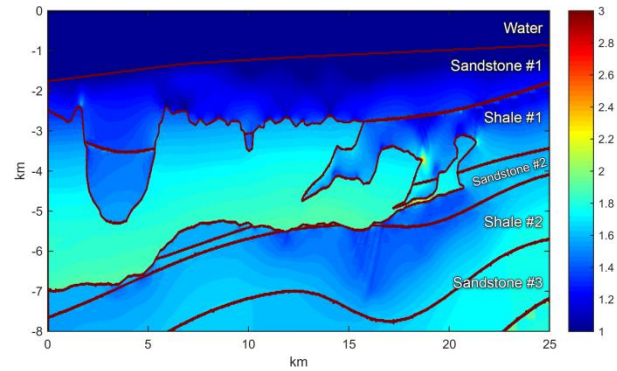


Figure 4.6 Magnitudes of principal total stress S_3 around the salt #2 (sg)

The S_1 , S_2 and S_3 are the maximum, intermediate and minimum principal total stresses, respectively. Reorientation of faulting regimes around salt structures are shown on Figure 4.7 and Figure 4.8. Cyan represents the normal stress regime. The strike-slip regime is represented by orange color. Reverse regime does not exist in this 2D geomechanical model. As salt, acts like a fluid on geological time scale, all principal stresses are almost identical (Nikolinakou et al., 2012). Because of this, the specific faulting regimes cannot exist in the salt structure. Green represents a transit regime zone.

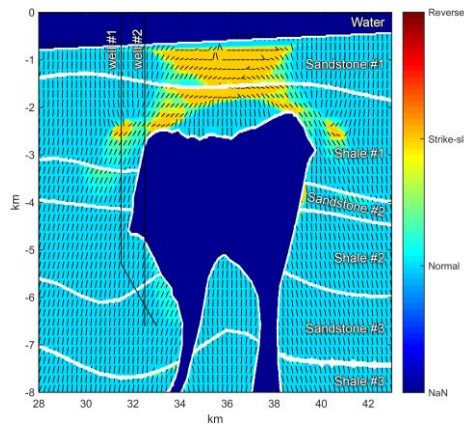


Figure 4.7 Faulting regimes and direction of principal total stress S_1 around the salt #1

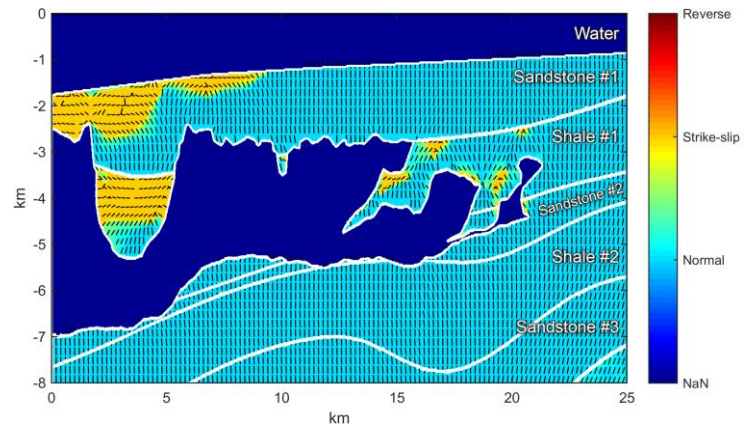


Figure 4.8 Faulting regimes and direction of principal total stress S_1 around the salt #2

4.2 Principal total stresses along wellbore trajectories

In this section calculations for the magnitude of principal stresses along wellbore trajectories are presented.

There are two wells in the model (see Figure 4.9).

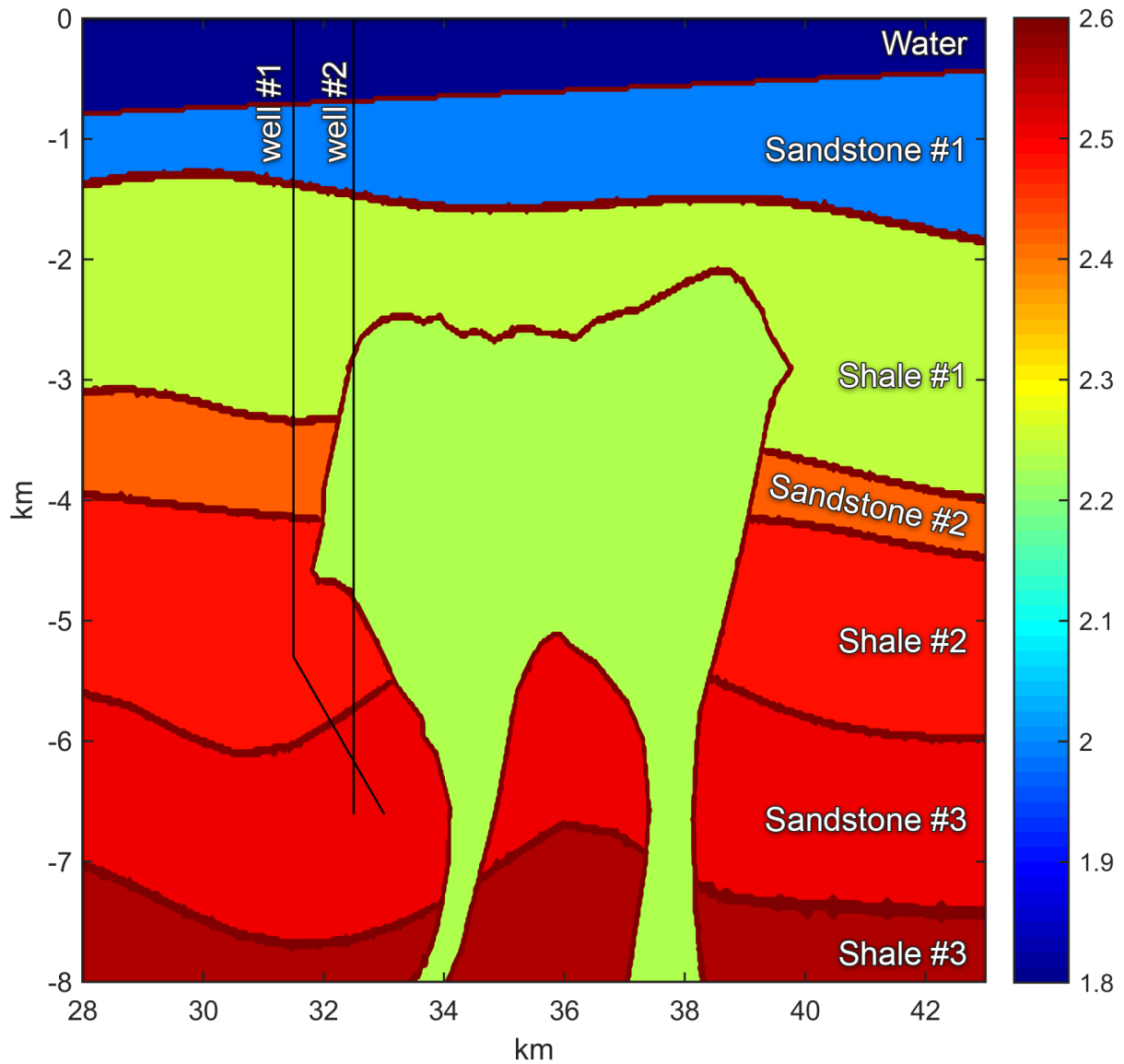


Figure 4.9 Density model around the salt #1 (sg)

Magnitudes of the principal total stresses along wellbore trajectories are shown in Figure 4.10 and Figure 4.11, for well #1 and well #2, respectively. The magnitudes of the principal stresses and the initial pore pressure are presented in the sg units. The pink curve on figure represents the principle stress S_1 . The red and blue curves show the magnitudes of principle stresses S_2 and S_3 . The green curve represents the initial pore pressure gradient. The stress plot from the wells is obtained from 2D geomechanical model by interpolation of results along wellbore trajectory.

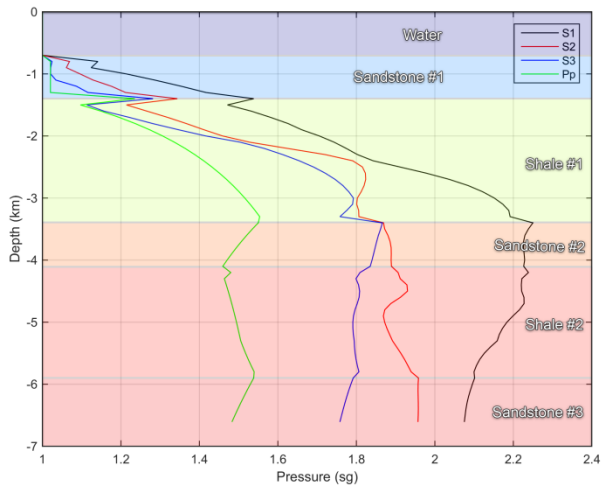


Figure 4.10 Magnitudes of principal total stresses and pore pressure along the well #1 (sg)

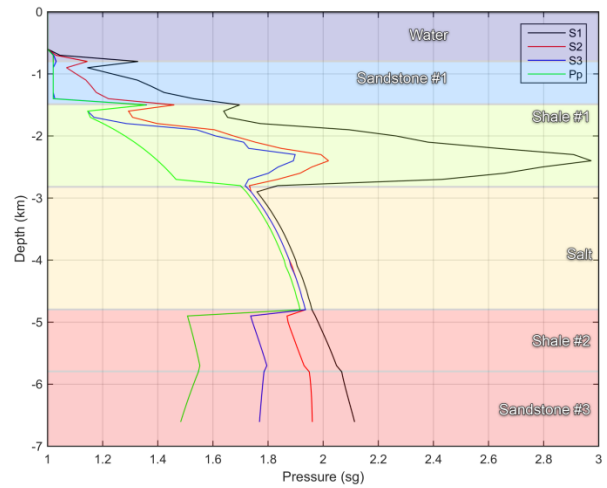


Figure 4.11 Magnitudes of principal total stresses along the well #2 (sg)

The well #2 passes through the salt formation at the depth from 2.9 km to 4.8 km. As the salt non-porous material at depth, pore pressure in salt structures is not defined. However if the inclusions of sediments are encountered in salt then the pore pressure could be close to overburden stress, normally considered as 97% of overburden stress (Fjar et al., 2008). Also for the well #2, principal total stresses in the salt are similar, because the salt does not have shear stresses.

5 Discussion of the results

In this section we discuss different overburden calculation methods, base on 2D Finite Element method, 1-D method and 2-D method. Vertical stress for the 1-D and 2-D methods was calculated using density interpolation performed in Matlab.

5.1 Comparison of the overburden stress calculated by the 2-D method and the Finite element method

In Figure 5.1, Figure 5.2, Figure 5.3 and Figure 5.4 the overburden stress calculation of finite element method (S_1) and 2-D method (S_{2D_v}) are demonstrated as follows:

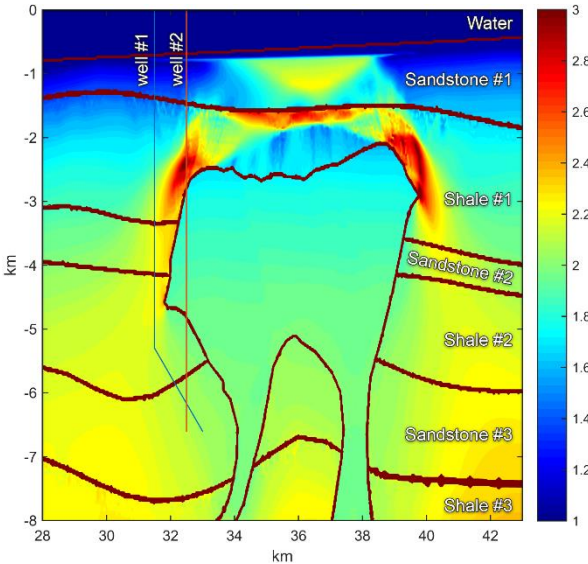


Figure 5.1 Magnitudes of maximum principal total stress S_1 calculated by Plaxis around the salt #1 (sg)

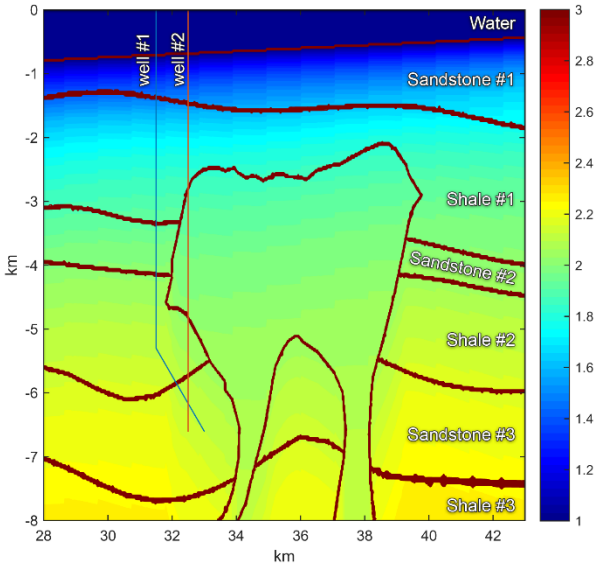


Figure 5.2 Magnitudes of vertical stress $S_{2D.v}$ calculated by 2D method around the salt #1 (sg)

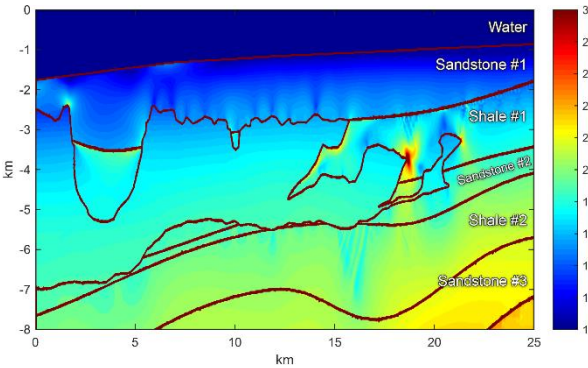


Figure 5.3 Magnitudes of maximum principal total stress S_1 calculated by Plaxis around the salt #2 (sg)

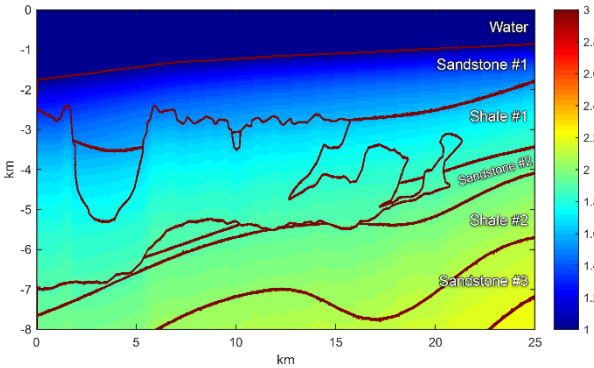


Figure 5.4 Magnitudes of vertical stress $S_{2D.v}$ calculated by 2D method around the salt #2 (sg)

By comparing the Figure 5.1 with Figure 5.2 and Figure 5.3 with Figure 5.4 easy to notice that the distribution of the vertical stress, in comparison with maximum principal total stress, is more uniform.

The comparison is calculated by subtracting the stress calculated from the finite element method and the stress obtained from the summation of the overlying rock weight at the same point (5.1).

$$\Delta S = S_1 - S_{2D_V} \tag{5.1}$$

Where ΔS is difference between overburden stresses at point in sg, and S_1 and S_{2D_V} are stresses at that point calculated by finite element method and by 2D method respectively in sg unit. Figure 5.5 shows the difference between overburden stresses.

The color in Figure 5.5, Figure 5.6, shows the different of magnitude of the overburden stress in the sg units. Red contours show the boundary of the formations on the figures.

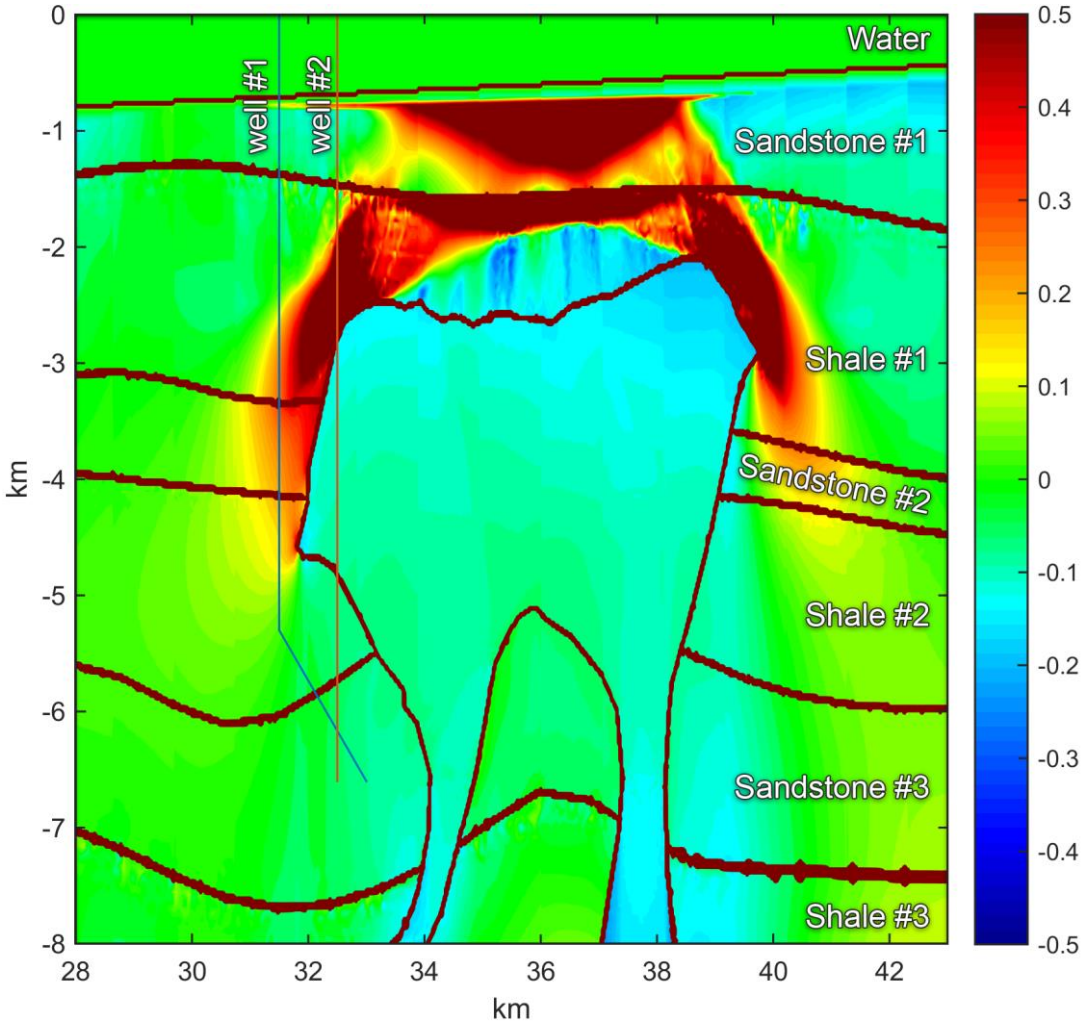


Figure 5.5 Difference between 2D and FEM overburden stress calculations around the salt #1 (sg)

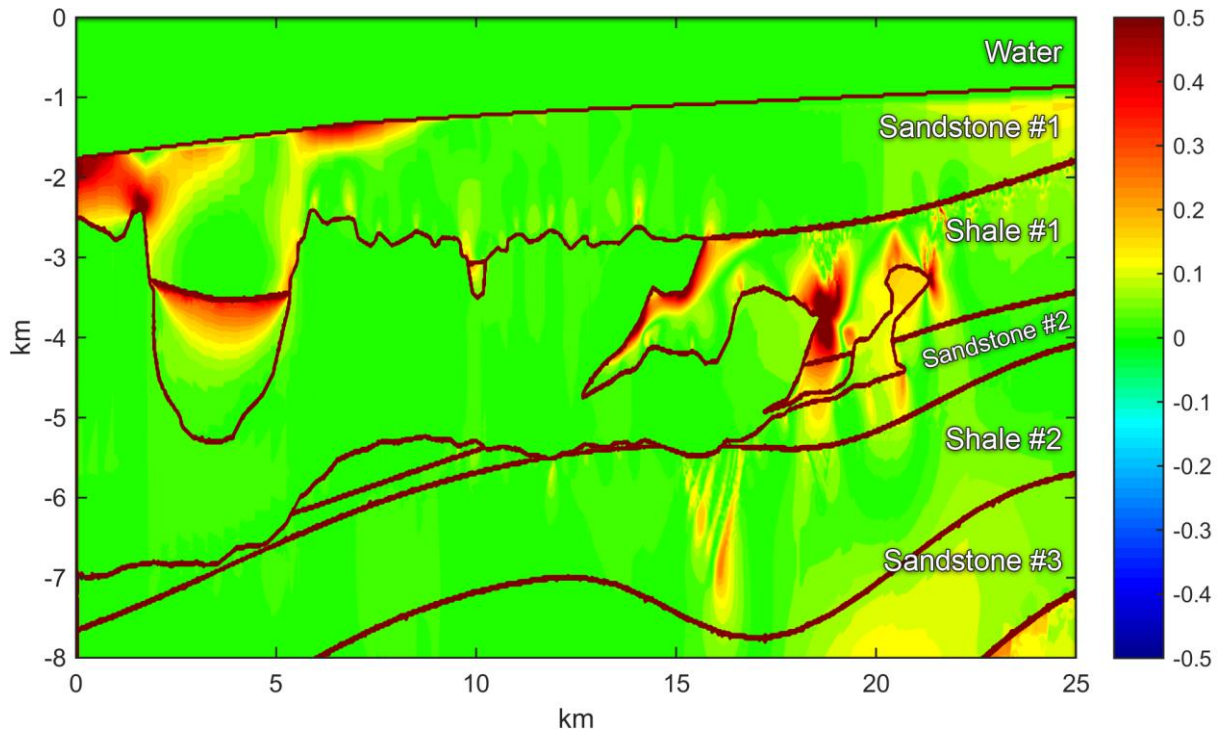


Figure 5.6 Difference between 2D and FEM overburden stress calculations around the salt #2 (sg)

Figure 5.5 and Figure 5.6 display a big difference between 2-D method and Finite element method near the sharp corners of salt borders. Red colors show areas where $S_1 > S_{2D_V}$; green colors show areas where $S_1 = S_{2D_V}$ and blue colors show areas where $S_1 < S_{2D_V}$. The difference between these methods near the sharp corners of the salt boundaries is associated with the fact that 2-D method does not predict stress concentrations near salt structures.

5.2 Comparison between the overburden stress calculated by the 2-D method and the 1-D method

Figure 5.7 and Figure 5.8 show the dependence of overburden stresses along wells estimated using different calculation methods. The blue curve on Figure 5.7 and Figure 5.8 represents the 1-D method, the red curve shows the 2-D method and the green curve represents the Finite Element method.

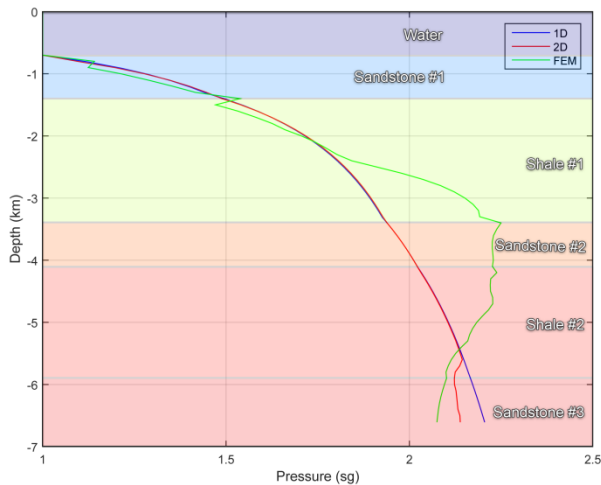


Figure 5.7 Magnitudes of maximum principal stress along the wellpath #1 for three calculation methods

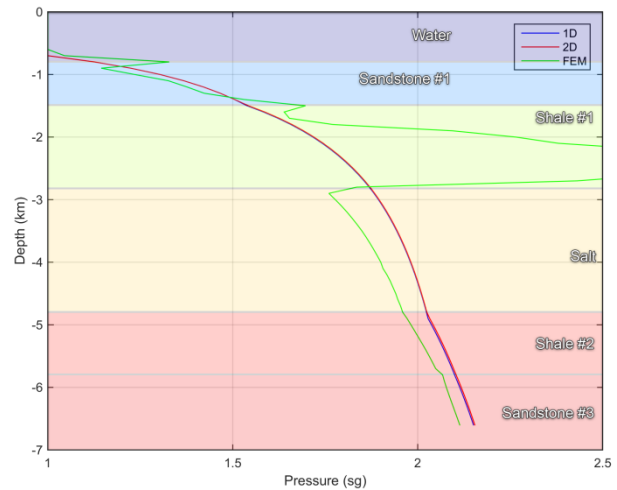


Figure 5.8 Magnitudes of maximum principal stress along the well-path #2 for three calculation methods

At the well #1 (see Figure 5.7) on the inclination section (from 5.5km to 6.7km) can be seen the deviations between the 1D and 2D methods of the overburden stress calculation. By comparing the 1D and 2D methods on Figure 5.7 and Figure 5.8, it can be concluded that the 2D methods is more appropriate for inclined boreholes, because the density above borehole may not be the same as density along wellbore. While 2D density integration method does not take into account the redistribution of stresses inside and outside of salt structures, which may significantly deviate from regional stress directions and magnitudes.

5.3 Advantages and disadvantages of methods which is used for creating the geomechanical model

1D method is a simplest method for calculating the overburden stress, which has many drawbacks. One of the main problems of this method is that it disregards the shape of the overlying layers. Another problem of this method is that it does not consider the effect of the stress direction.

2D method shows the better results than the 1D method. This method, as well as the previous method, does not consider the effect of the stress direction. Therefore, the vertical stress is coincided with a maximum principal stress at a distance from salts (see Figure 5.10). However, it gives wrong results around the salt boundaries.

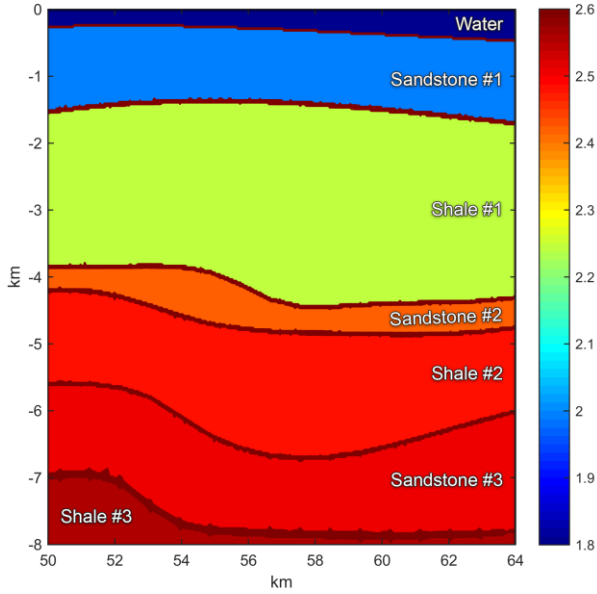


Figure 5.9 Density model at a distance from salts (sg)

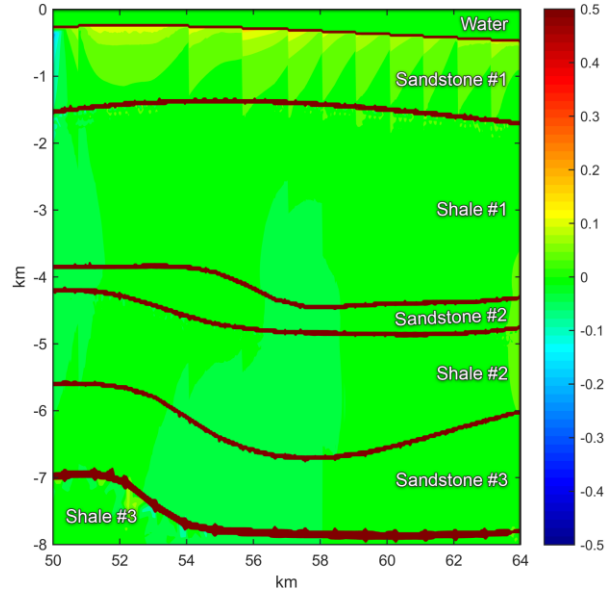


Figure 5.10 Difference between 2D and FEM overburden stress calculations at a distance from salts (sg)

In contrast to the previous methods, the finite element method provides a highly accurate prediction of magnitudes and directions of stresses (Fredrich et al., 2003), but the setting and calculations of the simulation model takes some time. In any case, this time and money are less than the time and money spent on the elimination of accident consequences (Alberty et al., 2004).

5.4 Pore pressure calculated by Bower's method

In addition, the effect of overburden calculation method on pore pressure prediction is shown on Figure 5.11 and Figure 5.13. These figures illustrate a comparison between two cases of pore pressure calculations.

1st case uses the maximum principal stress from Plaxis.

$$P_{P_{S1}} = S_1 - \left(\frac{V_P - V_{ml}}{A} \right)^{\frac{1}{B}} \quad (5.2)$$

In the 2nd case the vertical stress is used, which is calculated in Matlab

$$P_{P_{2D_V}} = S_{2D_V} - \left(\frac{V_P - V_{ml}}{A} \right)^{\frac{1}{B}} \quad (5.3)$$

ΔP_P shows a difference between the pore pressures.

$$\Delta P_P = P_{P_{S1}} - P_{P_{2D_V}} \quad (5.4)$$

Color scale has values in the range from -0.3 to 0.3. Green color represents a zero difference. Values above or below are shown in red and blue colors respectively. Sandstone layers have a grey solid because the Bower's method can be applicable only for shale calculation.

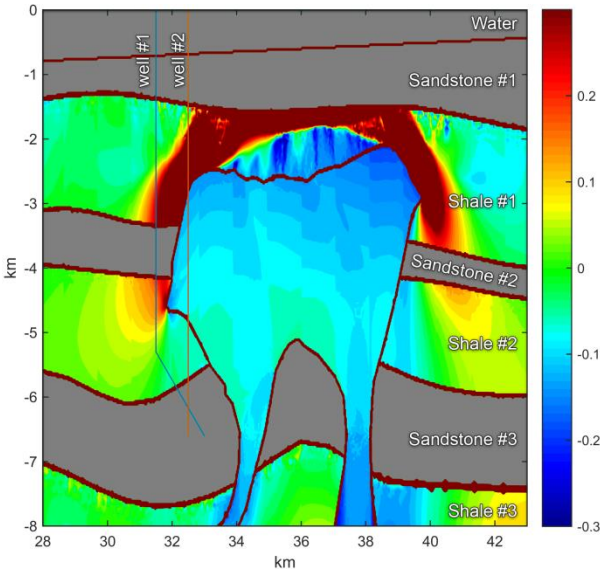


Figure 5.11 Difference between the pore pressure calculations in the salt #1 area (sg)

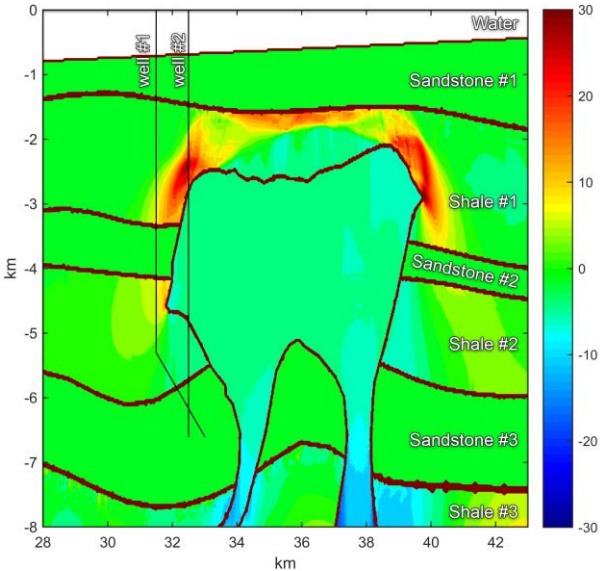


Figure 5.12 Difference between the pore pressure calculations in the salt #1 area (MPa)

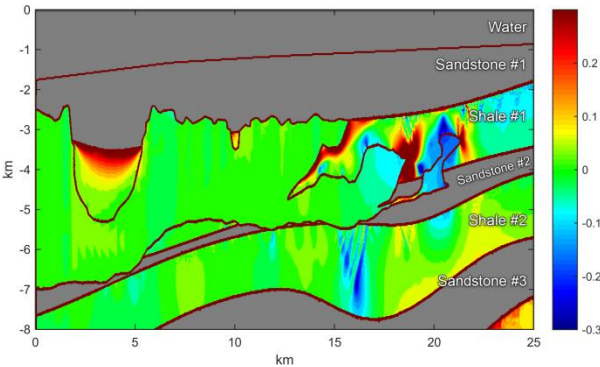


Figure 5.13 Difference between the pore pressure calculations in the section #2 (sg)

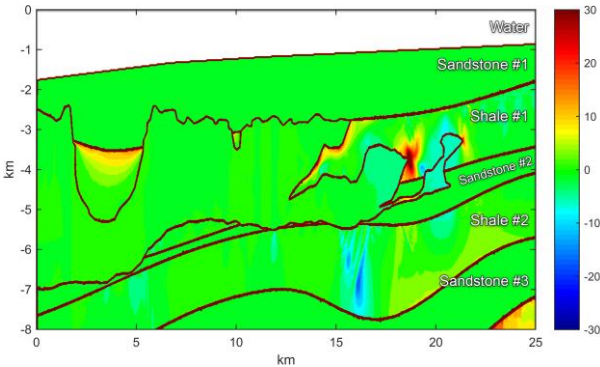


Figure 5.14 Difference between the pore pressure calculations in the section #2 (MPa)

See equation (5.4) for details

The results, which are presents on Figure 5.11 and Figure 5.13, demonstrate a difference of the pore pressure, which is calculated by using two different value of overburden stress. Red colors show areas where $P_{P_{S1}} > P_{P_{2D,V}}$; green colors show areas where $P_{P_{S1}} = P_{P_{2D,V}}$ and blue colors show areas where $P_{P_{S1}} < P_{P_{2D,V}}$. In some areas, the difference is more than 0.3sg. Predicted pore pressure in salt is also different, because pore pressure in sediment inclusion in salt is dependent on calculated overburden stress.

Figure 5.15 and Figure 5.16 show the dependence of difference between the pore pressures around the wells from the TVD.

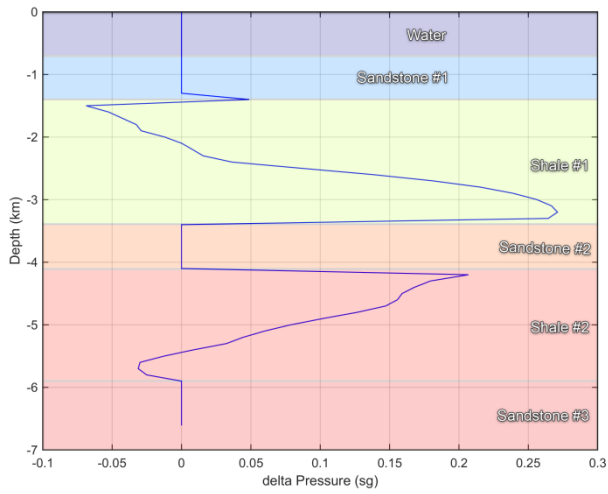


Figure 5.15 Difference between the pore pressure calculations in the well #1

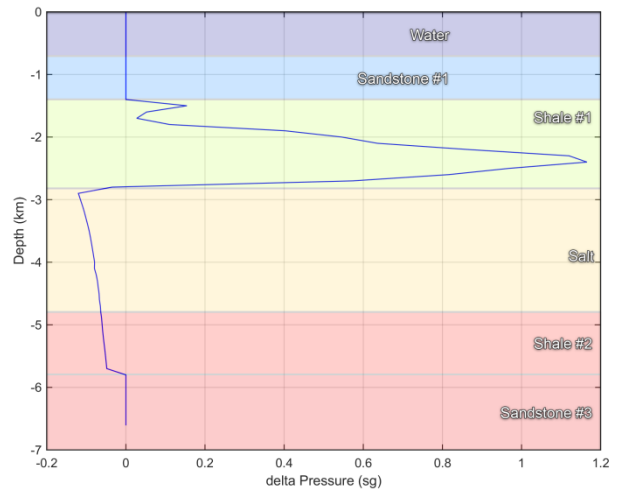


Figure 5.16 Difference between the pore pressure calculations in the well #2

The maximum difference of pore pressure in wells are 0.27 sg for well #1, and 1.19 sg for well #2.

6 Conclusions

In this master thesis, we created the geomechanical 2D model by the finite element method from synthetic 2D velocity model using empirical correlations developed for Gulf of Mexico and Plaxis software. Behavior of stresses in the sediments around the salt bodies was simulated. We received the quantitative difference in pore pressure and overburden stress predictions in a salt-related basin calculated with different methods, such as: a standard density integration and finite element modeling using Plaxis software.

Simulation results by Plaxis show that the high stress concentrations can be in the salt regions. It is connected with a re-orientation of stress near the salt structures, because the salt structure has a viscous nature and behaves like a fluid on geological time scale (Dusseault et al., 2004). Results of comparison demonstrate a big difference between finite element method and density integration method for calculation of overburden stress. In some areas, the difference is more than 2 sg. It leads to errors in pore pressure prediction with magnitude up to 30 MPa, if the density integration method is used. Subsequently, catastrophic accident, such as kick or blowout, may occur.

Also, in Gulf of Mexico, the pre-drill pore pressure cannot be exactly predicted without finite element modeling, because the salt structures spread in the whole area of Gulf of Mexico (Talbot, 1993).

It is also possible to come to the following conclusions from the obtained results:

- If geological model of the field have a salt structures, it is strongly recommended to make a simulation model for the calculations of stresses. Otherwise wellbore stability problem may occur, that will lead to loss the time and money. If one cannot perform the simulation, the Blowout preventer must be selected with a safe margin over at least 30MPa or more.
- For other cases, a 2-D or 1-D methods may be used, with the following restrictions: 1-D method can be applied to overburden calculation only for vertical wells; for deviated wells and horizontal wells 2-D method may be applied.

References

- Aadnoy, B., & Looyeh, R. (2011). Petroleum rock mechanics: drilling operations and well design.
- Alberty, M. W., & McLean, M. R. (2004). *A physical model for stress cages*. Paper presented at the SPE Annual Technical Conference and Exhibition.
- Anderson, E. M. (1951). *The dynamics of faulting and dyke formation with applications to Britain*: Hafner Pub. Co.
- Bathe, K. J. (2008). *Finite element method*: Wiley Online Library.
- Billette, F., & Brandsberg-Dahl, S. (2005). *The 2004 BP velocity benchmark*. Paper presented at the 67th EAGE Conference & Exhibition.
- Biot, M., & Willis, D. (1957). The theory of consolidation. *J. Appl Elastic Coefficients of the Mech*, 24, 594-601.
- Bly, M. (2011). *Deepwater Horizon accident investigation report*: Diane Publishing.
- Bradley, W. B. (1978). *Bore hole failure near salt domes*. Paper presented at the SPE Annual Fall Technical Conference and Exhibition.
- Bringgreve, R., & Vermeer, P. (1998). PLAXIS-finite element code for soil and rock analysis, version 7. *Plaxis BV, The Netherlands*.
- Brinkgreve, R. (2005). *Selection of soil models and parameters for geotechnical engineering application*. Paper presented at the Soil Constitutive Models@ sEvaluation, Selection, and Calibration.
- Brinkgreve, R., Kumarswamy, S., Swolfs, W., Waterman, D., Chesaru, A., Bonnier, P., & Haxaire, A. (2015). PLAXIS 2015.
- Carlson, D. H., Plummer, C. C., & McGeary, D. (2008). *Physical geology: Earth revealed*: McGraw-Hill.
- Castagna, J. P., Batzle, M. L., & Eastwood, R. L. (1985). Relationships between compressional-wave and shear-wave velocities in clastic silicate rocks. *Geophysics*, 50(4), 571-581.
- Cavalca, M., Fletcher, R., & Du, X. (2015). *Q-compensation through depth domain inversion*. Paper presented at the 77th EAGE Conference and Exhibition 2015.
- Chang, C., Zoback, M. D., & Khaksar, A. (2006). Empirical relations between rock strength and physical properties in sedimentary rocks. *Journal of Petroleum Science and Engineering*, 51(3), 223-237.
- Charlez, P. A. (1999). *The concept of mud weight window applied to complex drilling*. Paper presented at the SPE Annual Technical Conference and Exhibition.
- Darley, H. C., & Gray, G. R. (1988). *Composition and properties of drilling and completion fluids*: Gulf Professional Publishing.
- Dodson, J., Dodson, T., & Schmidt, V. (2004). Gulf of Mexico'trouble time'creates major drilling expenses: Use of cost-effective technologies needed. *Offshore*, 64(1).

- Dusseault, M. B., Maury, V., Sanfilippo, F., & Santarelli, F. J. (2004). *Drilling around salt: risks, stresses, and uncertainties*. Paper presented at the Gulf Rocks 2004, the 6th North America Rock Mechanics Symposium (NARMS).
- Eaton, B. A. (1969). Fracture gradient prediction and its application in oilfield operations. *Journal of petroleum technology*, 21(10), 1,353-351,360.
- Fjar, E., Holt, R. M., Raaen, A., Risnes, R., & Horsrud, P. (2008). *Petroleum related rock mechanics* (Vol. 53): Elsevier.
- Fredrich, J. T., Coblenz, D., Fossum, A. F., & Thorne, B. J. (2003). *Stress perturbations adjacent to salt bodies in the deepwater Gulf of Mexico*. Paper presented at the SPE Annual Technical Conference and Exhibition.
- Fredrich, J. T., Engler, B. P., Smith, J. A., Onyia, E. C., & Tolman, D. (2007). *Pre-drill estimation of sub-salt fracture gradient: analysis of the Spa prospect to validate non-linear finite element stress analyses*. Paper presented at the SPE/IADC Drilling Conference.
- Gardner, G., Gardner, L., & Gregory, A. (1985). Formation velocity and density: the diagnostic basics for stratigraphic traps. *Geophysics*, 50(11), 2085-2095.
- Gholami, R., Moradzadeh, A., Rasouli, V., & Hanachi, J. (2014). Practical application of failure criteria in determining safe mud weight windows in drilling operations. *Journal of Rock Mechanics and Geotechnical Engineering*, 6(1), 13-25.
- Glossary.oilfield.slb.com. (2016a). Poisson's ratio Retrieved from http://www.glossary.oilfield.slb.com/en/Terms/p/poissons_ratio.aspx
- Glossary.oilfield.slb.com. (2016b). Mud density. Retrieved from http://www.glossary.oilfield.slb.com/Terms/m/mud_density.aspx
- Haimson, B., & Cornet, F. (2003). ISRM suggested methods for rock stress estimation—part 3: hydraulic fracturing (HF) and/or hydraulic testing of pre-existing fractures (HTPF). *International Journal of Rock Mechanics and Mining Sciences*, 40(7), 1011-1020.
- Hubbert, M. K., & Willis, D. G. (1972). Mechanics of hydraulic fracturing.
- Huffman, A. R. (2002). The future of pore-pressure prediction using geophysical methods. *The Leading Edge*, 21(2), 199-205.
- Luo, G., Nikolinakou, M. A., Flemings, P. B., & Hudec, M. R. (2012). Geomechanical modeling of stresses adjacent to salt bodies: Part 1—Uncoupled models. *AAPG Bulletin*, 96(1), 43-64.
- Matthews, W., & Kelly, J. (1967). How to predict formation pressure and fracture gradient. *Oil and Gas Journal*, 65(8), 92-106.
- Mavko, G., Mukerji, T., & Dvorkin, J. (2009). *The rock physics handbook: Tools for seismic analysis of porous media*.
- McLean, M., & Addis, M. (1990). *Wellbore stability: the effect of strength criteria on mud weight recommendations*. Paper presented at the SPE Annual Technical Conference and Exhibition.
- Moos, D., Peska, P., Finkbeiner, T., & Zoback, M. (2003). Comprehensive wellbore stability analysis utilizing Quantitative Risk Assessment. *Journal of Petroleum Science and Engineering*, 38(3-4), 97-109. doi:[http://dx.doi.org/10.1016/S0920-4105\(03\)00024-X](http://dx.doi.org/10.1016/S0920-4105(03)00024-X)

- Nikolinakou, M. A., Hudec, M. R., & Flemings, P. B. (2014). Comparison of evolutionary and static modeling of stresses around a salt diapir. *Marine and Petroleum Geology*, *57*, 537-545.
- Nikolinakou, M. A., Luo, G., Hudec, M. R., & Flemings, P. B. (2012). Geomechanical modeling of stresses adjacent to salt bodies: Part 2—Poroelastoplasticity and coupled overpressures. *AAPG Bulletin*, *96*(1), 65-85.
- Paterson, M. S., & Wong, T.-f. (2005). *Experimental rock deformation-the brittle field*: Springer Science & Business Media.
- Rocscience.com. (2016). Strength Type. Retrieved from https://rocscience.com/help/slide/webhelp/slide_model/materials/Strength_Type.htm
- Røste, T., Dybvik, O. P., & Søreide, O. K. (2015). Overburden 4D time shifts induced by reservoir compaction at Snorre field. *The Leading Edge*, *34*(11), 1366-1374.
- Rozhko, A., Podladchikov, Y., & Renard, F. (2007). Failure patterns caused by localized rise in pore-fluid overpressure and effective strength of rocks. *Geophysical Research Letters*, *34*(22).
- Rozhko, A., Brevik, I., Thompson, N., & Søreide, O. K. (2014). Optimization of wellbore trajectory for hydraulic fracture operation below salt. *Statoil internal "Well Informed" magazine for drilling and well(#2)*.
- Sayers, C., Johnson, G., & Denyer, G. (2002). Predrill pore-pressure prediction using seismic data. *Geophysics*, *67*(4), 1286-1292.
- Talbot, C. (1993). Spreading of salt structures in the Gulf of Mexico. *Tectonophysics*, *228*(3), 151-166.
- Ti, K. S., Huat, B. B., Noorzaee, J., Jaafar, M. S., & Sew, G. S. (2009). A review of basic soil constitutive models for geotechnical application. *Electronic Journal of Geotechnical Engineering*, *14*, 1-18.
- Whitson, C. D., & McFadyen, M. K. (2001). *Lessons learned in the planning and drilling of deep, subsalt wells in the deepwater Gulf of Mexico*. Paper presented at the SPE Annual Technical Conference and Exhibition.
- Willson, S., Edwards, S., Heppard, P., Li, X., Coltrin, G., Chester, D., . . . Cocalles, B. (2003). *Wellbore stability challenges in the deep water, Gulf of Mexico: case history examples from the pompano field*. Paper presented at the SPE Annual Technical Conference and Exhibition.
- Willson, S. M., & Fredrich, J. T. (2005). *Geomechanics considerations for through-and near-salt well design*. Paper presented at the SPE Annual Technical Conference and Exhibition.
- Zhang, J. (2011). Pore pressure prediction from well logs: Methods, modifications, and new approaches. *Earth-Science Reviews*, *108*(1), 50-63.
- Zhang, J. (2013). Borehole stability analysis accounting for anisotropies in drilling to weak bedding planes. *International Journal of Rock Mechanics and Mining Sciences*, *60*, 160-170.
- Zhang, J., Standifird, W. B., & Lenamond, C. (2008). *Casing ultradeep, ultralong salt sections in deep water: a case study for failure diagnosis and risk mitigation in record-depth well*. Paper presented at the SPE Annual Technical Conference and Exhibition.

Zienkiewicz, O. C., & Taylor, R. L. (2005). *The finite element method for solid and structural mechanics*.

Zoback, M. D. (2010). *Reservoir geomechanics*: Cambridge University Press.

Appendix A. Definitions of the stress

Stress is the key element of solid mechanics. In order to determine the state of stress at one point in the Earth's crust, a shear tensor is used.

The components of the stress tensor can be separated into two categories. Each of components has a magnitude and orientation. The first category includes normal stresses (σ_{11} , σ_{22} , σ_{33}). Which act perpendicularly to the three orthogonal planes of the Cartesian coordinate system (see Figure A.1a), which define a Cartesian coordinate system (x_1 , x_2 , x_3). The second category contains shear stresses (τ_{12} , τ_{21} , τ_{13} , τ_{31} , τ_{23} , τ_{32}). In which forces are applied parallel the plane in a particular direction (Aadnoy et al., 2011). In the standard deformation theory, the stress tensor is symmetrical, consequently $\tau_{12} = \tau_{21}$, $\tau_{13} = \tau_{31}$ and $\tau_{23} = \tau_{32}$. Due to this stress tensor symmetry the number of stress components reduced to six.

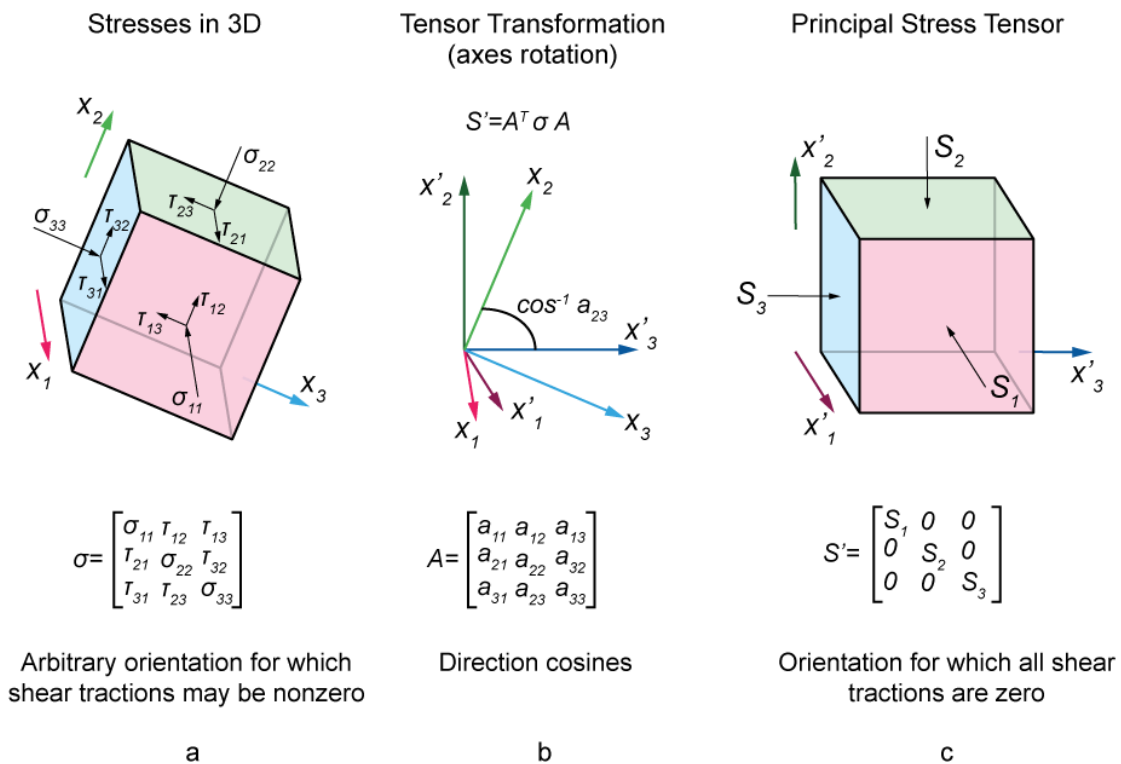


Figure A.1 (a) Stress tensor in Cartesian coordinates; (b) Tensor transformation through direction cosines; (c) The principal stress axes.

At each point there is a principal stress. Principal stresses are stresses, which act along the directions (x'_1 , x'_2 , x'_3) for which all shear stress components are zero (see Figure A.1c).

Transformation between the arbitrarily oriented stress tensor to the principal stress tensor, occurs through the rotation tensor. (Aadnoy et al., 2011)

Appendix B. Mohr Coulomb model

The Mohr Coulomb model is a simple and applicable to two-dimensional stress space mathematical model that describes the dependence of the shear stresses of the material on the applied normal stress (Brinkgreve et al., 1998). This model is an elastic-perfectly plastic model, which is often used to model soil behavior in general and serves as a first-order model (Ti et al., 2009) with a fixed yield surface, i.e. a yield surface that is fully defined by model parameters and not affected by (plastic) straining (Brinkgreve et al., 2015).

The basic Mohr-Coulomb model requires five input parameters (Brinkgreve et al., 2015). There are two defining parameters from Hooke's law Hooke's law: Young's modulus, E , and Poisson ratio, ν . Cohesion (c) and friction angle (ϕ) are parameters, which define the failure criteria. The flow rule is described by the angle of dilatancy (ψ).

They can be determined from the basic core test.

I. Young's modulus (E) and Poisson's ratio (ν)

In the Mohr-Coulomb model, Plaxis as the main stiffness parameters uses the Young's modulus and Poisson's ratio.

Young's modulus is a mechanical property of material, which describes the resistance of material to stretching / compression during the elastic deformation (Aadnoy et al., 2011). The parameter characterizes the degree of stiffness of the material. Young's modulus mathematical expression is shown below:

$$E = \frac{\sigma}{\varepsilon} \quad (\text{B.1})$$

Where E is Young's modulus, σ is tensile stress, and ε is extensional strain. Young's modulus tends to increase with increasing the pressure. Because of that, deep soil layers have greater stiffness than shallow layers.

Poisson's ratio is the ratio of the relative transverse contraction to the relative longitudinal extension. Poisson coefficient has values for isotropic materials from 0 to 0.5.

The value of the Young's modulus and Poisson's ratio can be obtained from the triaxial test of soil samples, or from the velocity log (Aadnoy et al., 2011).

Poisson's ratio and Young's modulus of fully describe the elastic properties of an isotropic material.

II. Cohesion (C), friction angle (ϕ) and angle of dilatancy (ψ)

Angle of dilatancy is a ratio between the rate of volumetric strain and the rate of shear strain (Aadnoy et al., 2011). For common geology cases it is equal to 0.

Cohesion is the component of shear strength of a rock or soil that is independent of interparticle friction. It affects the shear strength of a rock (Aadnoy et al., 2011).

Friction angle is another shear strength parameter of the soil. It describes the friction shear resistance of soils (Aadnoy et al., 2011).

Figure B.1 shows the Mohr-Coulomb failure criterion. The Mohr-Coulomb failure line (red color) is a visual representation of effect of cohesion and friction angle parameters on the strength of a rock.

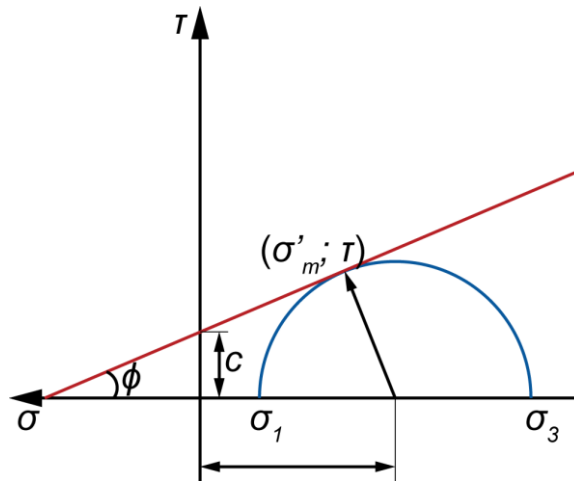


Figure B.1 Mohr-Coulomb failure criterion

In nature, rocks are porous materials consisting of a rock matrix and a fluid. Laboratory triaxial experiments show that the Mohr-Coulomb failure criterion is expressed as (Paterson et al., 2005; A. Rozhko et al., 2007):

$$\tau = C \times \cos \phi + \sigma'_m \times \sin(\phi) \quad (\text{B.2})$$

Where

$$\sigma'_m = \frac{\sigma_1 + \sigma_3}{2} - p \quad (\text{B.3})$$

is the mean effective stress, τ is the shear stress, c the cohesion of the material, and ϕ is the material angle of friction.